FACULTY OF TECHNOLOGY

EFFECTS OF BIOFUEL-DERIVED IMPURITIES ON NH_3-SCR CATALYST ACTIVITY AND DEACTIVATION

Tytti Ristikaarto

ENVIRONMENTAL ENGINEERING

Master's Thesis

February 2026

TIIVISTELMÄ

Biopolttoaineperäisten epäpuhtauksien vaikutus NH_3-SCR katalyytin aktiivisuuteen ja deaktivoitumiseen

Tytti Ristikaarto

Oulun yliopisto, Ympäristötekniikan tutkinto-ohjelma

Diplomityö, 2026, 96 s. ja 1 liite

Työn ohjaajat yliopistolla: Mika Huuhtanen TkT, Teuvo Maunula prof., TkT.

Tässä diplomityössä tutkittiin biopohjaisista polttoaineista peräisin olevien epäpuhtauksien vaikutusta Fe-pohjaisten SCR-katalyyttien aktiivisuuteen ja kestävyyteen Kokeellinen osuus keskittyi Fe-SCR Beta -zeoliittikatalyyttiin, jossa selvitettiin rikin, alkalimetallien (Na, K, Ca) ja fosforin yhteisvaikutuksia näiden katalyyttien aktiivisuuteen ja kestävyyteen.

Katalyyttien aktiivisuutta arvioitiin NO_X-, NH_3- ja N_2O-konversiomittauksilla, ja rakenteellisia muutoksia analysoitiin DRIFTS-, BET-, XRD- ja SEM–EDS-menetelmillä. Katalyyttien deaktivoituminen johtui aktiivisten katalyyttipaikkojen myrkyttymisestä ja mikrohuokoisen pinta-alan vähenemisestä. Myrkytettyjen näytteiden aktiivisuusjärjestys oli K > Ca > S > P > Na. Natrium ja fosfori aiheuttivat voimakkaimman deaktivoitumisen heikentämällä aktiivisuutta ja vähentämällä zeoliitin mikrohuokoisuutta, kun taas kalium ja kalsium eivät vaikuttaneet aktiivisuuteen yhtä merkittävästi.

Asiasanat: Bio-pohjaiset polttoaineet; Beta-zeoliitti; Fe-SCR; katalyytin deaktivoituminen; rikkimyrkytys; katalyyttimyrkyt

ABSTRACT

Effects of Biofuel-derived Impurities on NH_3-SCR Catalyst Activity and Deactivation

Tytti Ristikaarto

University of Oulu, Degree Programme in Environmental Engineering

Master's thesis, 2026, 96 pp. and 1 Appendix

Supervisors at the university: Mika Huuhtanen D.Sc.(Tech.), Teuvo Maunula Prof. of Practice, D.Sc.(Tech.)

This Master's thesis investigates the deactivation of Fe-based SCR catalysts exposed to impurities originating from bio-based fuels. The study focuses on Fe-SCR catalysts supported on Beta zeolite and examines the combined effects of sulphur, alkali metals (Na, K, Ca) and phosphorus on catalytic performance and structural stability.

Catalyst activity was evaluated through NO_X, NH_3 and N_2O conversion measurements, while structural and surface changes were analysed using DRIFTS, BET, XRD and SEM–EDS. Deactivation was found to result from catalyst site poisoning and a loss of microporous surface area. The catalyst activity ranking of poisoned samples was K > Ca > S > P > Na. Sodium and phosphorus caused the strongest deactivation by suppressing catalyst activity and reducing zeolitic microporosity, whereas potassium and calcium do not have so significant impact.

Keywords: Bio-based fuels; catalyst deactivation; Fe-SCR; sulphur poisoning; zeolite Beta; catalyst poisons

ACKNOWLEDGEMENTS

This work was carried out as part of the Flex-CPT project co-funded by Business Finland. I gratefully acknowledge the financial support provided by the project and its funding partners, which made this research possible.

I would like to express my sincere gratitude to my supervisors, Mika Huuhtanen and Teuvo Maunula, for their guidance and support throughout this work. I thank Mika for welcoming me into the project and for his excellent supervision, encouraging attitude, and warm support, as well as his strong academic expertise in catalysis research. I thank Teuvo for bringing an invaluable industry perspective and decades of experience in emission catalyst technology. I greatly appreciate both my supervisors for our practical discussions, constructive atmosphere, and shared sense of humour, which made this work both productive and enjoyable.

I would also like to thank my colleagues Kaisu Ainassaari, Laura Annunen, Jaakko Petrelius and Riikka Help for their support. I thank Kaisu for assistance with BET measurements, and Laura for guidance in laboratory practices and peer support. I especially thank Jaakko, whose collaboration during this project has grown into a valued friendship. I also thank Riikka for her kindness and encouragement. I extend my thanks to the entire ECE research group for providing an inspiring and supportive working environment.

I am grateful to my friends Inka Malila, Fanni Koskela, and Aamu Mykkänen for their peer support and welcome distractions during my studies, and to Emma Holappa and Axel Selmgren for their long-standing friendship and emotional support. A special thank you goes to Anette Kassinen for her steadfast presence and support over the years.

My deepest gratitude goes to my husband, Mikael Multasuo, for his constant support, patience, and care throughout this journey. I also thank my parents, Päivi Ristikaarto and Jyrki Pelasoja, for their unconditional support and for shaping me into who I am today. It is clear, that not even single line of this thesis would have been written without you. Finally, I thank my sister Tiia Ristikaarto and my cousin Jenna Ristikaarto, whose friendship and encouragement have meant more to me than words can express.

Oulu, 11.02.2026

Tytti Ristikaarto

Tytti Ristikaarto

TABLE OF CONTENTS

LIST OF SYMBOLS AND ABBREVIATIONS

BET	Brunauer-Emmet-Teller
BJH	Barrett-Joyner-Halenda
CAGR	Compound Annual Growth Rate
CaSHT	Calsium-sulphur hydrotreated
DRIFTS	Diffuse Reflectance Infrared Fourier Transform Spectroscopy
DPF	Diesel Particulate Filter
DOC	Diesel Oxidation Catalyst
EEA	European Environment Agen
EU	European Union
EPA	Environmental Protection Agency
FER	Ferrierite
GHG	Greenhouse gas
GHSV	Gas Hourly Space Velocity
HT	Hydrotreatment
KSHT	Potassium-sulphur hydrotreated
MOR	Mordenite
NaSHT	Sodium-sulphur hydrotreated
NO_X	Nitrogen Oxides
PM	Particulate Matter
PSHT	Phosphorus-sulphur hydrotreated
RED III	Renewable energy directive III
SHT	Sulphur hydrotreated
SCR	Selective catalyst reduction
SEM-EDS	Scanning Electron Microscopy and Energy Dispersive X-ray Spectroscopy
TWC	Three-way catalyst
USD	United States Dollar
XRD	X-ray Diffraction
ZDDP	Zinc Dialkyldithiophospate
γ-alumina	gamma-aluminium
γ-Al_2O_3	gamma-aluminium

1 CATALYTIC PERSPECTIVES ON BIO-BASED FUELS IN THE GLOBAL ENERGY TRANSITION

1.1 Background and importance

Due to the environmental crisis posed by climate change, there is a global shift toward achieving carbon neutrality. The energy sector is responsible for approximately 73 percent of global greenhouse emissions (IEA 2023), making it a key focus area for transitioning away from fossil fuels. For instance, the European Union has set a target to be carbon neutral by the year 2050 as a part of its European Green Deal (European Commission 2020). As part of this transition, the Renewable Energy Directive (RED III, Directive (EU) 2023/2413) sets binding targets for renewable energy deployment and defines sustainability criteria for biofuels, bioliquids and biomass fuels within the EU (European Parliament and Council 2023). As a result, the demand for alternative fuels to replace fossil-based ones is expected to increase significantly in the coming decades. Potential alternatives include, such as, green hydrogen, synthetic fuels, and bio-based fuels. In addition to reducing greenhouse gas emissions, the transformation of the energy sector is also crucial for ensuring energy security and self-sufficiency, as well as for enhancing resilience, supporting local eco_{no}mies, and fostering technological information. In the future, the global energy landscape will increasingly comprise diverse energy sources. For example, Finland's national energy strategy emphasizes the use of multiple renewable energy sources, with key sources being wind power, hydro power, biomass and solar energy (Ministry of Economic Affairs and Employment of Finland 2022).

Regulatory frameworks play a key role in supporting this transition. The European Union's Renewable Energy Directive (RED III) sets mandatory sustainability criteria and minimum greenhouse gas (GHG) savings threshold for biofuels and bioliquids used in transport and heating. These ensure that bio-based fuels contribute to genuine emission reductions without causing deforestation or other adverse environmental impacts (Directive (EU) 2023/2413). Additionally, standards such as EN 15940 for paraffinic diesel fuel define quality parameters to guarantee long-term performance, safety and compatibility with modern engines (EVS 2023).

Durability requirements are also central to regulatory oversight. Both the U.S. Environmental Protection Agency (EPA) and the European Environment Agency (EEA) mandate that emission control systems, including catalytic converters, retain their effectiveness throughout the operational lifespan of engines of industrial processes (EPA 2014; EEA 2021). In addition, the new Euro 7 regulatory framework explicitly introduces durability requirements for emission control systems over extended vehicle lifetimes (ICCT 2024). Similarly, biofuels must exhibit chemical and thermal stability over extended storage periods and usage cycles to comply with quality assurance frameworks such as European Committee for Standardization (CEN) fuel specifications. Examples of such standards include EN 14214 for biodiesel and EN 15940 for paraffinic diesel, which define physicochemical stability and storage requirements (CEN 2023; EVS 2023).

Bio-based fuels represent one class of alternative fuels and are utilized in power generation, transportation, and industrial processes. Bio-based fuels are derived from biomass, including vegetable oils, agricultural residues, forestry and wood-processing by-products, food waste, microalgae, and other advanced feedstocks. (Cavelius et al. 2023; Padder et al. 2024.) Bio-based fuels are commonly categorized as first-, second-, third-generation biofuels. First-generation biofuels are produced from edible feedstocks such as corn or sugarcane. An example of first-generation biofuel is bioethanol. (Padder et al. 2024.) In contrast, second-generation biofuels are derived from non-edible waste materials and residues, such as straw and forest residues. These fuels offer the advantage of not competing with food production. (Jeswani et al. 2020.) Third-generation biofuels, which are currently under development, show significant potential for sustainable production and are based primarily on high-yield sources such as microalgae (Cavelius et al. 2023; Padder et al. 2024). The key advances of bio-based fuels include their renewability, compatibility with existing fuel distribution infrastructure, and their lower net carbon dioxide emissions relative to conventional fossil fuels (IEA 2021). However, to ensure these benefits are realized in practice, compliance with emissions, durability, and sustainability regulations is essential.

Catalysts are materials that facilitate chemical reactions by lowering activation energies and directing the reactions toward desired products. They play a crucial role in modern industrial chemistry, with estimates suggesting that “more than 85 % of all chemical products are manufactured with the help of catalysts” (Heveling 2012). Their role is critical from an environmental perspective in today’s global world, where environmental

crises such as climate change pose potential future threats. From an economic perspective, catalyst enhances process efficiency by reducing material, energy, and time requirements, thereby lowering operational costs (Isahak & Al-Amiery 2024).

However, catalytic processes are not without challenges, one of which is deactivation. Deactivation refers to the gradual decline in catalyst activity over time, which can diminish projects efficiency and result in formation of chemical waste due to loss of active sites and fouling phenomena (Forzatti & Lietti 1999; Anekwe 2025). This presents significant environmental and economic drawbacks. Bio-based fuels often contain impurities such as sulphur, nitrogen compounds, and metals that can adversely affect catalyst activity, stability and tolerance because these heteroatom contaminants can poison active sites and accelerate deactivation mechanisms (Pham et al. 2024; Lin et al. 2022).

Emission catalysts, such as diesel oxidation catalysts (DOC), selective catalytic reduction (SCR) and three-way catalysts (TWC), are particularly sensitive to fuel quality. Regulatory bodies therefore require durability testing of these systems to ensure long-term compliance with emission standards such as Euro 6/7 in the EU and EPA Tier 3 in the U.S. These frameworks impose strict limits on nitrogen oxides (NO_x), carbon monoxide (CO), hydrocarbons (HC), and particulate matter (PM) emissions, reinforcing the importance of both clean fuel inputs and robust catalytic technologies. (European Commission 2021; EPA 2023.)

1.2 Objectives of the work

This study examines the fundamental characteristics of SCR catalysts, including the change of their structure and functional properties by deactivation. Special emphasis is placed on catalyst chemical deactivation, its various mechanisms, and the broader implications of deactivation from both environmental and economic viewpoints. The study also reviews the potential of catalyst regeneration and the requirements for successful recovery of catalytic activity. The materials and methods employed in the experimental section of this work are described in detail in a dedicated chapter. The overarching objective of this thesis is to examine how impurities present in bio-based fuels influence the activity, properties, and durability of catalysts. The work seeks to

identify the types and extent of catalyst deactivation encountered. Catalyst poisoning and surface interactions are investigated using advanced characterization methods, such as Brunauer-Emmet-Teller (BET), Scanning Electron Microscopy with Energy Dispersive X-ray Spectroscopy (SEM-EDS), and Diffuse Reflectance Infrared Fourier Transform Spectroscopy (DRIFTS), which provide insights into catalyst morphology, elements compositions and adsorbed species on surface.

2 EMISSION CATALYSTS AND THEIR DEACTIVATION

Catalyst is a material which enhances chemical reactions by providing an alternative reaction pathway with a lower activation energy. Ideally, catalysts themselves are not consumed in reaction. (Richardson 1989) Catalysis refers to a process, in which a catalyst facilitates the desired chemical reaction. This study focuses specifically on emission catalysts.

2.1 Catalyst structure and properties

Usually, catalysts consist of three different kinds of components. These components are called active components, a support (or "carrier"), and promoters. These components are distinct, and they serve different roles in the catalytic system. (Richardson 1989)

The active component is responsible for catalytic activity and is the key driver of the chemical reaction. Selecting the active component is usually the first step in designing catalysts. It also determines the catalyst's selectivity, which influences the yield of the desired product. Active compounds are often metals, oxides or/and sulphides. (Richardson 1989) In automotive emission control catalysts, platinum group metals (PGMs), platinum (Pt), palladium (Pd), and rhodium (Rh), remain the essential active components due to their unique oxidation and reduction properties. Platinum is widely applied in diesel oxidation catalysts (DOCs) and three-way catalysts (TWCs). (Heck et al. 2002; Twigg 2011; Russell & Epling 2011.) Palladium has become increasingly dominant in gasoline TWCs, particularly under stoichiometric and transient cold-start conditions where high concentrations of CO and hydrocarbons are present. Studies highlight that Pd exhibits strong hydrocarbon oxidation activity and improved hydrothermal stability in modern high-temperature gasoline exhaust environments (Russell & Epling 2011; Kim et al. 2021). The increasing reliance on Pd has also been driven by fluctuating PGM market prices and advances in Pd-rich catalyst formulations (Kim et al. 2021). Rhodium remains indispensable for NO_X reduction under stoichiometric or slightly rich conditions due to its superior selectivity toward N_2 formation and its ability to dissociate NO efficiently (Heck et al. 2002; Twigg 2011). Despite its very low crustal abundance and high cost, no alternative metal has yet matched Rh performance in three-way catalysts (Kim et al. 2022). These three metals are typically

employed together in so-called TWC, which simultaneously promote the oxidation of carbon monoxide and hydrocarbons, as well as the reduction of nitrogen oxides in vehicle exhaust gases (Twigg 2007). Their high catalytic activity, resistance to deactivation, and thermal stability make them well-suited for harsh exhaust conditions despite their high cost (Burch 2010).

Vanadium, copper and iron are widely used as active components in selective catalytic reduction (SCR) systems targeting nitrogen oxide emissions (Ye et al. 2022). The most common active components in diesel oxidation catalysts (DOCs) are platinum and palladium dispersed on high-surface-area supports such as gamma-aluminium oxide (γ–alumina, $\gamma–Al_2O_{3)}$ as a main compound. Platinum exhibits high activity for both CO and HC oxidation, particularly at lower exhaust temperatures, and strong NO oxidation capability, which is beneficial for downstream systems. Palladium offers complementary HC oxidation activity and thermal stabilisation, making Pt-Pd combinations common in commercial DOC formulations to balance activity, durability, and cost. (Koebel et al. 2000; Russell and Epling 2011.)

The support component serves several important functions. Primarily, it provides a high surface area for the active component, which facilitates more effective catalytic reactions on the surface. A high porosity is generally required for this. In addition, the support provides structural stability, mechanical strength, and can influence the properties of the active component. Common support materials include high-porosity metal oxides, zeolites, clays or carbon. (Richardson 1989.) In emission catalysts, the most widely used support material is γ–alumina, which provides a large surface area and thermal resistance, promoting good dispersion of active metal particles and enhancing exposure to exhaust gases (Twigg 2007). Cerium oxide, or ceria, (CeO_2) is also commonly used, not only as a support but also as a promotor due to its oxygen storage and release capacity, which helps balance the oxidation and reduction environment within the catalyst. Zirconium oxide is frequently combined with ceria to improve thermal stability and structural integrity. (Li et al. 2016.) Although perovskite-type oxides have been studied as promising alternatives due to their redox properties and resistance to thermal degradation, their commercial application in emission catalysts have remained limited (Burch 2010).

As Richardson (1989, p.35) explains:" A promoter is some third agent which when added, often in small amounts, results in desirable activity, selectivity or stability effects."

Promoters are typically added to enhance the function of either the active component or the support component. For instance, promoters might be added to the support component to reduce unwanted side reactions, such as coke formation. In vanadia-based NH_3-SCR catalysts, promoters such as tungsten oxide (WO_3) and molybdenum oxide (MoO_3) are widely incorporated with TiO_2 to enhance catalytic performance by increasing surface acidity, stabilising active vanadium oxide species, broadening the effective temperature window, and improving resistance to deactivation under practical exhaust conditions (Zhang et al. 2019). Lanthanum oxide (La_2O_3) is used to stabilize γ-alumina supports by suppressing phase transformation at high temperatures, improving long-term thermal durability (Li et al. 2016). Silicon oxide (SiO_2) is commonly incorporated into alumina supports to reduce sintering and preserve surface area under hydrothermal aging (Gao et al. 2016b). Promoters may also inhibit coke formation or improve oxygen mobility in redox catalysts (Richardson 1989).

Catalysts come in a variety of shapes and structures, each designed to meet specific needs in chemical processes. Common catalyst forms include pellets, honeycombs, extrudates, spheres, granules, flakes, and powders. (Richardson 1989). In emission control, monolithic honeycomb catalysts are the dominant form due to their low pressure drop and high geometric surface area (Twigg 2007). Honeycomb monoliths contain parallel channels that provide uniform gas flow distribution and short external diffusion distances to catalytic surfaces (Govender & Friedrich 2017). Ceramic honeycombs made from cordierite offer excellent thermal shock resistance, while metallic honeycombs provide superior thermal conductivity, thin walls and mechanical strength (Meißner et al. 2023). These shapes affect directly the catalyst's performance, durability, and cost. Generally, catalysts composed of smaller particles tend to be more expensive because they require more precise manufacturing and material handling (Richardson 1989; Ravindran & Madhu 2020; Ulusoy 2023). For example, pellets are made by compressing powdered material in a pelleting press, resulting in dense, uniform cylindrical particles. These are widely used due to their balance of surface area and mechanical strength. Extrudates are formed by pushing a paste through a die and cutting it into shapes, sometimes complex ones like trilobes, which improve surface area and gas flow. They are strong and common in fixed-bed reactors. Spheres, often made by spray drying, work well in fluidized beds due to their smooth flow and durability. Granules and flakes are less uniform and more economical, and they are often used in simpler processes. Powders, the finest form,

provide a high surface area but are harder to handle in many reactors. (Richardson 1989; Ravindran & Madhu 2020.) Catalyst particle shape and structural design play a critical role in durability and long-term performance. Mechanically robust forms such as extrudates and spherical pellets exhibit improved resistance to attrition and crushing, while tailored pore architecture enhances mass transport and mitigates fouling or pore blockage during operation (Farrauto & Bartholomew 2006; Twigg 2007; Ravindran & Madhu 2020). Together, these features help extend catalyst life by reducing common deactivation issues (Richardson 1989).

In addition to these particulate catalyst forms, monolithic catalysts are the mainstream in processes requiring low pressure drop and high geometric surface area, like emission catalysts. They are widely used in environmental processes such as automotive exhaust treatment, selective catalytic reduction, volatile organic compound destruction, catalytic combustion and preferential oxidation of carbon monoxide. Monoliths are usually ceramic or metallic honeycomb substrates. They are coated with a porous washcoat containing the above-mentioned porous support, active catalyst and promoters to increase total surface area and dispersed expensive active metals even to reach high reactivity, mass transfer and heat transfer. (Govender & Friedrich 2017.) Metal substrated monoliths have a thin layer of support and active metal deposited directly on a thin metallic foil (Meißner et al. 2023).

Catalytic performance depends not only on intrinsic reaction kinetics but also on efficient mass transfer of reactants to active sites (Fogler 2016). In porous catalysts, reactants must diffuse through boundary layers and internal pore networks before reaching active sites (Ravindran & Madhu 2020). In the case diffusion is slow compared to reaction rate, the mass-transfer limitations reduce overall effectiveness (Fogler 2016). In monolithic honeycomb catalysts, gas-phase mass transfer occurs from bulk flow to channel walls (external diffusion), followed by diffusion through the washcoat to active sites (internal/pore diffusion) (Govender & Friedrich 2017). Thin washcoat layers and high porosity are therefore essential to minimize diffusion resistance (Meißner et al. 2023). Optimized pore networks ensure efficient access of reactants to catalytic sites while allowing rapid removal of products, thereby maintaining high reaction rates (Fogler 2016).

According to Richardson (1989), the key catalyst properties include activity, selectivity, stability, durability, mechanical strength and porosity. Activity refers to how effectively a catalyst accelerates the desired reaction, while selectivity describes its ability to favour specific products. Stability is crucial for maintaining performance over time despite exposure to poisons, fouling, or sintering. Durability reflects how susceptible a catalyst is to changes in operating conditions or deactivating agents. Mechanical strength ensures that a catalyst can withstand physical stresses during use, and porosity affects how easily reactants can access active sites. Richardson highlights that optimizing a catalyst requires balancing these interrelated properties to suit the specific process needs.

2.2 Types of emission catalysts

Emission catalysts are engineered materials designed to facilitate chemical reactions that convert harmful exhaust gas constituents into less harmful species by lowering activation energy barriers for surface reactions. Their effectiveness depends primarily on the chemical environment of the exhaust and the specific pollutants targeted for conversion. (Heck et al. 2012; Sandhu et al. 2024.)

The design and functionality of emission catalysts are influenced by the stoichiometry of the combustion process. Under stoichiometric conditions, oxidation and reduction reactions can proceed concurrently due to balanced oxygen availability, whereas under oxygen-rich (lean) conditions, alternative catalytic strategies are required to effectively reduce nitrogen oxides (Twigg 2007; Sandhu et al. 2024). Modern catalyst research emphasizes improving temperature windows and selectivity to ensure high conversion efficiency during both cold start and dynamic transient operation (Sandhu et al. 2024).

In addition to reaction pathways, catalyst materials possess high thermal stability and resistance to deactivation mechanisms such as sintering and poisoning by trace exhaust components. Elevated exhaust temperatures and contaminants like sulphur can degrade catalyst performance over time, which has spurred research into more robust materials and formulations. (Bartholomew 2001; Maunula et al. 2025.) Materials optimization aims to enhance light-off behaviour, long-term durability, and resistance to changes in fuel composition (Heck et al. 2012; Maunula et al. 2025).

Emerging concerns related to next-generation fuels, including hydrogen, ammonia, and biofuels, have further motivated development of flexible aftertreatment catalysts capable of coping with broader exhaust compositions without sacrificing activity or durability (Maunula et al. 2025). These considerations underscore why different catalyst technologies must be tailored to specific engine types and operating regimes.

2.2.1 Selective Catalytic Reduction (SCR) Catalysts

Selective catalytic reduction (SCR) technologies are applied in diesel engine aftertreatment to reduce NO_X emissions through reactions with ammonia (NH_3), typically generated from injected urea solution (Koebel et al. 2000). SCR catalyst systems frequently employ vanadia–titania (V_2O_5–TiO_2) or zeolite-based materials such as Cu- or Fe-exchanged zeolites owing to their high hydrothermal stability and redox performance across a broad temperature range (Zhang et al. 2019; Jabłońska 2022). Effective catalyst performance depends on maintaining appropriate exhaust temperatures (typically 250–400 °C) and mitigating deactivation mechanisms such as sulphate poisoning and thermal sintering (Zhang et al. 2019). Cu-zeolites are the main SCR technology in the latest vehicle and machinery diesel applications since 2014, due to their hydrothermal durability, good low temperature activity (< 250°C) and a low dependency on NO_2 promotion. Fe-zeolites have been applied also for mobile applications due to their good high temperature activity (400–600°C) and low N_2O formation ability.

Fundamental reaction network of NH_3-SCR

In automotive selective catalytic reduction (SCR) systems, ammonia (NH_3) required for nitrogen oxides (NO_X) reduction is generated in situ from an aqueous urea solution. The process begins with urea thermolysis according to:

$$(NH_2)_2CO \rightarrow NH_3 + HNCO$$

This reaction is followed by the hydrolysis of isocyanic acid:

$$HNCO + H_2O \rightarrow NH_3 + CO_2$$

The overall reaction can therefore be written as:

$$(NH_2)_2CO + H_2O \rightarrow 2\,NH_3 + CO_2$$

Complete conversion of urea typically requires exhaust gas temperatures above approximately 180–200 °C, together with sufficient mixing and residence time. At lower temperatures, incomplete decomposition may result in the formation of solid by-products such as biuret or cyanuric acid, which can lead to deposit formation upstream of the SCR catalyst and negatively affect system performance (Koebel et al. 2000; Nova and Tronconi 2014).

When nitric oxide (NO) is the dominant NO_X species in the exhaust gas, the standard SCR reaction prevails:

$$4\,NH_3 + 4\,NO + O_2 \rightarrow 4\,N_2 + 6\,H_2O$$

This reaction is typically most effective within the temperature range of approximately 250–400 °C, depending on the catalyst formulation. It represents the principal pathway for NO reduction under NO-rich conditions, generally when the NO_2/NO_X ratio is below about 0.5. Both vanadia–titania catalysts and Cu- or Fe-exchanged zeolites exhibit high activity in this temperature window (Koebel et al. 2000; Zhang et al. 2019).

When NO and NO_2 are present in approximately equimolar concentrations ($NO_2/NO_X \approx 0.5$), the fast SCR reaction becomes dominant:

$$2\,NH_3 + NO + NO_2 \rightarrow 2\,N_2 + 3\,H_2O$$

This pathway is kinetically faster than the standard SCR reaction and is particularly beneficial at lower temperatures, typically between 200 and 350 °C. The enhanced rate is attributed to synergistic redox interactions between NO and NO_2 on the catalyst surface. In practical systems, the required NO_2 fraction is usually generated upstream in a diesel oxidation catalyst (DOC) via partial oxidation of NO. Optimizing the NO_2/NO_X ratio is therefore critical for achieving high low-temperature NO_X conversion efficiency (Koebel et al. 2000; Nova and Tronconi 2014; Jabłońska 2022).

Under NO_2-rich conditions ($NO_2/NO_X > 0.5$), the following net reaction may occur:

$$4\,NH_3 + 3\,NO_2 \rightarrow 3.5\,N_2 + 6\,H_2O$$

This pathway is often referred to as the "slow NO_2-SCR" reaction because its kinetics are generally less favourable than those of the fast SCR reaction. Consequently, precise control of the NO_2 fraction in the exhaust gas is essential for optimal SCR operation (Nova and Tronconi 2014; Zhang et al. 2019).

The oxidation of NO to NO_2 plays a key role in determining the relative contributions of the standard and fast SCR pathways:

$$2\,NO + O_2 \leftrightarrow 2\,NO_2$$

This reaction typically occurs over platinum-containing diesel oxidation catalysts positioned upstream of the SCR unit. By adjusting the NO_2 concentration, the system can be tuned to favour the fast SCR mechanism, particularly under low-temperature driving conditions (Koebel et al. 2000; Nova and Tronconi 2014).

At elevated temperatures, typically above 400–450 °C depending on the catalyst type, ammonia may undergo undesired oxidation reactions that compete with the SCR process. Selective oxidation to nitrogen proceeds according to:

$$4\,NH_3 + 3\,O_2 \rightarrow 2\,N_2 + 6\,H_2O$$

However, ammonia can also form nitrous oxide:

$$2\,NH_3 + 2\,O_2 \rightarrow N_2O + 3\,H_2O$$

or nitric oxide:

$$4\,NH_3 + 5\,O_2 \rightarrow 4\,NO + 6\,H_2O$$

These side reactions reduce the availability of NH_3 for NO_X reduction and may increase secondary emissions such as N_2O, a potent greenhouse gas. To minimize ammonia slip

and secondary pollutant formation, ammonia slip catalysts (ASC) are commonly installed downstream of the main SCR catalyst (Nova and Tronconi 2014; Zhang et al. 2019).

At low temperatures, particularly under NO_2-rich conditions, ammonium nitrate may form via nitric acid intermediates according to:

$$NH_3 + HNO_3 \leftrightarrow NH_4NO_3$$

Ammonium nitrate can accumulate within catalyst pores below approximately 200–250 °C, temporarily blocking active sites and decreasing catalytic activity. Upon heating, these deposits may decompose, restoring activity but potentially leading to transient N_2O formation (Nova and Tronconi 2014; Jabłońska 2022).

Sulphur-containing species in the exhaust gas can also affect SCR performance. Sulphur dioxide may be oxidized to sulphur trioxide:

$$SO_2 + \frac{1}{2}O_2 \leftrightarrow SO_3$$

Subsequently, sulphur trioxide can react with water and ammonia to form ammonium bisulphate or ammonium sulphate:

$$SO_3 + H_2O + NH_3 \rightarrow NH_4HSO_4$$

$$SO_3 + H_2O + 2\,NH_3 \rightarrow (NH_4)_2SO_4$$

These sulphate species may deposit on the catalyst surface and within pore structures, leading to pore blockage and masking of active sites. Sulphur poisoning is particularly relevant for vanadia-based catalysts and can significantly impair long-term durability (Koebel et al. 2000; Zhang et al. 2019).

The global market for selective catalytic reduction catalysts is experiencing steady growth, driven primarily by increasingly stringent emission regulations in the automotive, industrial, and energy sectors. Recent estimates value the SCR catalyst market at approximately USD 4.1–4.4 billion in 2022–2023, with projections reaching USD 6.2–6.7 billion by 2030–2032 at the compound annual growth rate (CAGR) of 4.6–5.5 %

(Verified Market Reports 2023; Dataintelo 2023). Technological advancements such as improved zeolite and vanadium-based catalysts, modular retrofitting designs, and compatibility with future hydrogen-fuel systems further contribute to market expansion by addressing durability and efficiency challenges (Mordor Intelligence 2024).

Iron-based zeolite catalysts

Iron-based zeolite catalysts have gained considerable attention as alternatives to conventional vanadium formulations for NH_3-SCR due to their broad operational temperature window, strong redox properties, and comparatively lower environmental impact. In Fe-zeolite systems (e.g., Fe-MOR, Fe-ZSM-5, Fe-Beta, and Fe-CHA), the Fe^{2+}/Fe^{3+} redox cycle plays a central mechanistic role: Fe^{2+} is oxidized to Fe^{3+} by O_2, enabling activation of NO or NO_2 and subsequent reaction with NH_3 to form N_2 and H_2O (Lai & Wachs 2018). Catalyst performance depends strongly on iron dispersion, oxidation-state distribution, support topology, and surface acidity (Li et al. 2022a). In addition, the Si/Al ratio of the zeolite framework governs hydrothermal stability, Brønsted acidity, and the anchoring environment of isolated Fe^{3+} cations. Higher Si/Al ratios generally enhance resistance to dealumination during hydrothermal aging, whereas excessively high ratios reduce the density of exchange sites and may lower low-temperature SCR activity (Gao et al. 2016a). Advanced spectroscopic studies demonstrate that isolated framework-associated Fe^{3+} species are generally more active than aggregated FeO_X clusters, which form during hydrothermal aging (Gao et al. 2013a; Chen et al. 2022). Consequently, optimal SCR performance requires a balance between framework stability and redox-site density (Li et al. 2022a).

Despite their favourable medium–high temperature activity, Fe-SCR catalysts face intrinsic challenges at low temperatures. Standard SCR over Fe-zeolites often relies on partial NO oxidation to access the fast-SCR pathway, making sufficient NO_2 availability critical for achieving high low-temperature conversion efficiencies (Lai & Wachs 2018; Li et al. 2022a; Gao 2020).

Fe-ZSM-5 was among the first extensively investigated systems for NH_3-SCR (Brandenberger et al. 2008). Its MFI framework stabilizes isolated Fe species at exchange sites, enabling efficient redox cycling in the 300–450 °C range. However, severe hydrothermal aging promotes dealumination and iron migration, leading to formation of

inactive FeO_X clusters and irreversible deactivation (Gao et al. 2013a; Schneider et al. 2021). To overcome these limitations, larger-pore BEA frameworks (Fe-Beta) were developed. The three-dimensional 12-membered-ring channel system enhances diffusion and improves stabilization of redox-active Fe species during hydrothermal aging (Gao et al. 2016b; Abdul Nasir et al. 2024). As a result, Fe-Beta exhibits a broader operational window and enhanced durability compared with Fe-ZSM-5 (Gao et al. 2016b).

Small-pore CHA-type zeolites such as SSZ-13 represent a further structural advancement. The double six-membered ring cages confine isolated Fe species and restrict migration during aging, limiting formation of large iron oxide particles (Li et al. 2022a; Gao 2020). This confinement effect contributes to improved retention of redox-active sites under severe hydrothermal treatment (Gao 2020).

Frameworks such as MOR and FER have also been investigated; however, their predominantly one-dimensional channel systems are more susceptible to pore blocking and diffusion limitations under aging conditions (Brandenberger et al. 2008; Schneider et al. 2021). For this reason, current catalyst development has largely focused on BEA and CHA topologies for improved structural robustness and long-term performance (Li et al. 2022a; Gao 2020).

Vanadium-based zeolite catalysts

Vanadium-based catalysts, typically V_2O_5-WO_5/TiO_2, remain the industrial benchmark for NH_3-SCR due to their excellent activity in the 300–400 °C range, long-term durability in high-SO_X conditions and established large-scale production (Ye et al. 2022). V-SCR catalysts have been the main SCR in power plant, marine and first (Euro 4-5 during 2005-2014) vehicle applications. The catalytic mechanism involves redox cycling between V^{5+} and V^{4+} species, where V^{5+} sites oxidize NO to NO_2, facilitating the “fast SCR” pathway, while ammonia adsorbed on acid sites participates in forming N_2 and H_2O (Lai & Wachs 2018). Recent research on VO_X/TiO_2 based SCR catalysts has focused on extending catalytic activity toward lower temperatures, improving resistance to H_2O and SO_2 poisoning through support and promoter design, and optimizing vanadium loading to balance activity, toxicity, and cost (Ye et al. 2022; Bian 2024; Zhang et al. 2024a). However, vanadium-based catalysts also face concerns regarding volatilization or leaching of V and W species under high-temperature or sulphur-rich conditions, raising

issues for catalyst longevity and environmental safety (Liu et al. 2015). As a result, current development trends centre on stabilisation strategies, improved supports, and hybrid catalysts formulations that maintain the robustness of V-SCR while mitigating its limitations.

Vanadium-based catalysts, usually V_2O_5 supported on TiO_2 and promoted with WO_3, are the most common choice in stationary applications. Industrial formulations typically contain 0.5–3 wt% V_2O_5, and 5–10 wt% WO_3, which provide high NO_X-removal (de-NO_X) efficiency, good sulphur and water tolerance, and robust performance in hydrocarbon and formaldehyde oxidation. (Ye et al. 2022)

Current mechanistic evidence indicates that dinuclear V-W ensembles can constitute particularly active sites for NO_2 -involved SCR pathways, offering higher intrinsic activity than isolated V species or V-V dimers, which helps explain activity/selectivity trends at practical vanadium oxide surface densities (Xu et al. 2023). Known trade-offs include a tendency of V-based systems to oxidize SO_2 to SO_3 (risking ammonium bisulphate formation with high-S fuels) and a narrower low-temperature window, which must be balanced by formulation and process design (Lai & Wachs 2018; Ye et al. 2022).

2.2.2 Diesel Oxidation Catalysts (DOCs)

Diesel oxidation catalysts (DOCs) are predominantly used in diesel engines to oxidize CO, HCs, and the soluble organic fraction of particulate matter. They typically use platinum (Pt) and palladium (Pd) dispersed on γ-alumina supports, offering high surface area and thermal durability. (Ho et al. 2021; Zhang et al. 2022.)

DOCs are generally placed upstream in aftertreatment systems, where they reduce CO and HC emissions and encourage partial formation of NO to NO_2, which is vital for diesel particulate filter (DPF) regeneration and SCR promotion. (Richardson 1989; Zhang et al. 2022). Developed Pt-Pd alloys also help resist sulphur poisoning and enhance oxidation performance (Ho et al. 2021).

2.2.3 Three-Way Catalysts (TWCs)

Three-way catalysts (TWCs) are employed in gasoline spark-ignition engines operating at near stoichiometric air-fuel ratios ($\lambda \approx 1$). The key to TWC performance is the dynamic performance between oxidation and reduction reactions with narrow λ-window, which enables simultaneous removal of CO, HCs, and NO_X with high efficiency. (Guillen-Hurtado et al. 2012; Rood et al. 2019.) Catalyst formulations often include Pt, Pd, and Rh deposited on ceria-promoted alumina supports, which aid in oxygen storage and improve kinetics in oscillating lambda conditions (Rood et al. 2019).

TWCs are typically implemented as monolithic honeycomb substrates coated with washcoats (support and active metals) containing platinum-group metals and ceria or ceria-zirconia for oxygen buffering (Guillen-Hurtado et al. 2012).

3 CATALYST DEACTIVATION

During operation, catalysts are subjected to thermal stress, reactive intermediates, and impurities that induce physicochemical transformations of the active phase and support. These transformations manifest as various deactivation pathways that limit activity, selectivity, and durability (Bartholomew 2001; Argyle and Bartholomew 2015). The underlying mechanisms differ depending on catalyst composition, structure, and reaction environment.

According to Richardson (1989), different deactivation processes (thermal, mechanical and chemical) may occur simultaneously and can vary significantly depending on catalyst composition, operating environment, and impurity exposure. Common deactivation mechanisms include poisoning by strongly adsorbed impurities, fouling or coking that blocks active sites, and sintering or thermal degradation that leads to loss of surface area and structural changes in the catalyst. These mechanisms ultimately reduce catalyst lifetime and process efficiency.

Recent literature has further emphasized these deactivation pathways and introduced modern approaches for mitigation and regeneration. Anekwe and Isa (2025) present a comprehensive review of chemical, thermal and mechanical deactivation mechanisms, highlighting poisoning, coking and thermal damage as dominant causes of activity loss. They also discuss contemporary regeneration technologies, such as oxidative and gasification treatments, plasma-assisted regeneration and surface modification techniques, aimed at restoring catalyst activity.

3.1 Thermal deactivation

Thermal deactivation refers to changes in the catalyst due to prolonged exposure to high temperatures. It is especially relevant in automotive and industrial catalysis, where fluctuating or extreme temperatures are common. (Richardson 1989; Anekwe & Isa 2025). In many catalytic systems, the most severe thermal deactivation occurs under so-called stoichiometric worst-case conditions, where temperatures can reach approximately 800–1000 °C. At these temperatures, irreversible transformations of both the active phase and the support may occur, drastically reducing catalytic performance. These

transformations include accelerated sintering, phase changes of support materials and loss of surface area. (Anekwe & Isa 2025).

Sintering involves the migration and coalescence of active metal particles, which leads to a decrease in active surface area and catalytic activity. This typically occurs under prolonged high-temperature conditions, especially in oxidative atmospheres where metal mobility increases (Richardson 1989; Väliheikki 2016 and references therein; Hansen et al. 2013; Honkanen et al. 2016). At elevated temperatures, catalyst supports may also undergo structural changes that reduce surface area and pore volume, thereby decreasing the dispersion of active species and limiting reactant accessibility to catalytic sites (Bartholomew 2001; Li et al. 2022b; Kaunisto et al. 2023).

In zeolite-based catalysts, such as Fe-exchanged zeolites used in NH_3-SCR applications, high-temperature and hydrothermal exposure can cause dealumination of the zeolite framework, loss of crystallinity and partial collapse of microporous structure, which directly reduces the number of isolated active Fe sites and lowers catalytic performance (Li et al. 2022b; Zhao 2021). These framework alterations are a major cause of thermal and hydrothermal deactivation in Fe-SCR catalysts operating under realistic exhaust conditions.

More generally, non-zeolitic oxide supports, such as alumina or mixed oxides, may undergo phase transformations and pore coarsening at high temperatures, leading to loss of surface area and mechanical stability (Kaunisto et al. 2023). Thus, both active phase sintering and support restructuring contribute significantly to long-term thermal deactivation of heterogeneous catalysts.

In the case of Fe-based SCR catalysts, thermal and hydrothermal deactivation is a significant challenge. Fe-SCR catalysts, such as Fe-exchanged zeolites (e.g., Fe-ZSM-5), typically show high NO_X conversion efficiency at moderate temperatures (150–450 °C), but repeated exposure to high exhaust temperatures and water vapor can lead to hydrothermal aging. During aging, migration and clustering of Fe species and partial loss of isolated active Fe sites may occur, resulting in decreased SCR activity (Brandenberger et al. 2011).

3.2 Mechanical deactivation

Mechanical deactivation results from physical damage or material loss, typically caused by stress, abrasion, or vibrations during operation. While less discussed in detail, it plays a significant role in catalyst degradation in mobile systems like automotive converters. (Richardson 1989; Anekwe & Isa 2025)

According to Richardson (1989), attrition involves the loss of catalytic material through friction or particle breakage. In fixed- or fluidized-bed systems, high flow rates can lead to erosion of catalyst particles or support structures. Similar erosion phenomena have also been observed in automotive catalyst washcoats under prolonged exhaust gas flow, contributing to gradual loss of active material (Koltsakis & Stamatelos, 1997; Heck et al. 2001).

Frequent and rapid temperature fluctuations in automotive systems cause thermal stress, which can lead to cracking, delamination or failures of the ceramic substrate or coating layer. Repeated vibration and thermal cycling further accelerate mechanical degradation. (Kröger 2007 and references therein; Kärkkäinen 2017 and references therein; Twigg 2014). In monolithic catalysts, the active washcoat may separate from the ceramic substrate due to thermal expansion mismatch or mechanical stress, which is a common failure mode in aged automotive catalysts (Richardson 1989; Heck et al. 2001).

In Fe-based SCR catalysts, mechanical stability is particularly important because Fe-zeolite washcoats are deposited on monolithic substrates and exposed to continuous exhaust flow, vibration and thermal cycling. Nova et al. (2014) report that in aged automotive SCR systems, repeated thermal cycling and exhaust pulsation can cause microcracking and partial detachment of the zeolite washcoat from the ceramic substrate, leading to gradual loss of active catalytic material. Liu et al. (2020) further show that prolonged operation under realistic driving conditions results in mechanical erosion and thinning of zeolite-based washcoats, which reduces the number of accessible Fe active sites and contributes to long-term SCR performance decline.

3.3 Chemical deactivation

Chemical deactivation arises from chemical interactions between the catalyst and components in the process gas, fuel or lubricants, leading to surface blocking, structural changes or irreversible transformations of active sites (Richardson 1989; Bartholomew 2001; Zhang 2024c). Recent reviews highlight that chemical deactivation remains one of the most significant causes of long-term performance loss in real automotive and industrial systems due to a combination of poisoning, fouling and framework damage (Zhang 2024b).

Poisoning involves strong and often irreversible binding of impurities to active sites, inhibiting catalytic reactions (Richardson 1989; Bartholomew 2001; Wang 2023). Sulphur and phosphorus are among the most significant poisons in automotive catalysts, typically originating from fuel or lubricants (Kröger 2007 and references therein; Kärkkäinen 2017 and references therein; Zhang 2024c). Sulphur poisoning in SCR systems has been confirmed experimentally to reduce catalyst activity by forming surface sulphates or sulphite species that block active sites and can shift redox equilibria unfavourably (Zhang 2024b). Phosphorus poisoning originates mainly from lubricant additives such as zinc dialkyldithiophospate (ZDDP), and phosphorus forms phosphate species on catalyst surfaces, blocking active sites and decreasing oxygen storage capacity (Kärkkäinen 2017 and references therein; Zhang 2024c). Lead and halogen (primarily chlorine and bromine) poisoning were historically caused by leaded gasoline and halide-containing fuels, leading to permanent noble metal deactivation, although their occurrence has declined due to fuel regulations (Kröger 2007 and references therein; Twigg 2014).

Fouling refers to deposition of inert materials such as carbonaceous residues, ash or lubricant-derived elements on catalyst surfaces, physically blocking pores and active sites (Väliheikki 2016 and references therein; Bartholomew 2001; Wei 2025). In automotive exhaust systems, oil-derived elements such as calcium, zinc and magnesium contribute significantly to ash fouling and pore blockage in catalyst washcoats, accelerating deactivation (Zhang 2024c).

Some catalysts also undergo chemical transformations under real operating conditions, including oxidation, reduction or sulfidation, which can alter surface structure and

reactivity (Väliheikki 2016 and references therein; Kärkkäinen 2017 and references therein; Bartholomew 2001). Hydrocarbon species and other exhaust components have also been shown to contribute to chemical pore blockage and selective poisoning in SCR catalysts under real driving conditions (Zhang 2024b).

In Fe-based SCR catalysts, chemical deactivation is strongly influenced by poisoning and fouling of zeolite active sites (Brandenberger et al. 2011; Wang 2023). State-of-the-art studies on zeolite SCR catalyst deactivation report that sulphur, phosphorus and alkali metal contaminants in exhaust gases cause progressive decline in NOx conversion efficiency by blocking acid sites and altering the zeolite framework (Wang 2023). Recent work also indicates that combined real-world poisoning factors in diesel exhaust can accelerate the deterioration of Cu- and Fe-zeolite SCR catalysts beyond what is seen in controlled laboratory aging (Zhang 2024b).

3.3.1 DOC-specific deactivation

Diesel oxidation catalysts (DOCs) are particularly vulnerable to chemical poisoning by sulphur- and phosphorus-containing compounds originating from fuel and lubricating oil additives. These species adsorb on active noble metal sites and form stable surface sulphates and phosphates, thereby blocking oxygen activation and inhibiting oxidation reactions of CO, hydrocarbons, and NO to NO_2 (Lietti et al. 1996; Lambert 2004; Wang et al. 2020; Yang et al. 2021). In Pt–Pd diesel oxidation catalysts, palladium is generally more sensitive to sulphur poisoning than platinum, leading to a more pronounced decline in hydrocarbon oxidation activity under sulphur-containing exhaust conditions (Russell & Epling 2011; Kim et al. 2021). Sulphur poisoning is especially critical under low-temperature conditions, where stable sulphate species form on the catalyst surface and strongly suppress catalytic activity until higher temperatures enable desulfation and activity recovery (Yang et al. 2021; Hamzehlouyan et al. 2016).

Phosphorus poisoning in automotive catalysts originates primarily from zinc dialkyldithiophosphate (ZDDP) lubricant additives, which thermally decompose during engine operation. The resulting phosphorus-containing species form stable metal phosphates that deposit on catalyst surfaces, blocking active noble metal sites and reducing their accessibility and overall catalytic performance (Theis et al. 2001). In addition to active site blocking, phosphorus species can react with oxide supports and

contribute to loss of specific surface area and pore blockage, leading to irreversible performance deterioration (Agote-Arán et al. 2023).

DOCs also function as the first component in multi-stage exhaust aftertreatment systems, strongly influencing the performance of downstream diesel particulate filters (DPFs) and selective catalytic reduction (SCR) units, as the oxidation of NO to NO_2 in the DOC promotes the fast SCR reaction pathway and enhances NO_X conversion efficiency (Chen et al. 2024). Therefore, DOC poisoning or deactivation has a system-level impact on overall emission control efficiency by reducing NO oxidation activity and subsequently impairing downstream SCR performance (Karre et al. 2023).

3.3.2 TWC-specific deactivation

Three-way catalysts (TWCs) operate under stoichiometric gasoline engine conditions that can produce exhaust gas temperatures typically ranging from 800 to 1000 °C. Under such severe thermal environments, thermal deactivation becomes the dominant aging mechanism, driven by sintering and agglomeration of noble metal particles as well as collapse of high-surface-area oxide supports (Kašpar et al. 2003; He & Wang 2016). Prolonged exposure to high temperatures leads to progressive thermal aging of three-way catalysts, promoting noble metal sintering and structural changes in ceria-based oxygen storage components. These processes reduce metal dispersion and significantly decrease oxygen storage capacity (OSC), thereby impairing both oxidation and reduction activity under stoichiometric operating conditions (Gong et al. 2019).

Phosphorus poisoning also significantly affects TWC performance. Phosphorus-containing species derived from lubricant additives react with alumina and ceria–zirconia supports to form thermally stable phosphate phases, such as $AlPO_4$ and $CePO_4$. The formation of these species decreases specific surface area and disrupts the Ce^{3+}/Ce^{4+} redox cycle, thereby impairing oxygen storage and release capacity (Theis et al. 2001). Because three-way catalysts rely simultaneously on the oxidation of CO and hydrocarbons and the reduction of NOx, degradation of the oxygen storage support with age directly compromises overall conversion efficiency (Gelmini et al. 2021; Sabatini et al., 2016). Additionally, interaction between thermal aging and chemical poisoning accelerates irreversible deactivation by promoting noble metal encapsulation and support densification (Zhao et al. 2021).

3.3.3 SCR-specific deactivation

Selective catalytic reduction (SCR) catalysts exhibit strong dependence on upstream exhaust conditions, particularly the NO/NO_2 ratio and ammonia availability. These parameters are significantly influenced by DOC activity, linking SCR efficiency to upstream catalyst performance (Kärkkäinen 2017 and references therein; Nova & Tronconi 2019). Deactivation mechanisms of SCR catalysts include thermal aging, hydrothermal sintering, sulphur poisoning, alkali metal contamination, and deposition of lubricant-derived phosphorus species (Zhang et al. 2019).

Hydrothermal aging at temperatures above 700 °C can lead to framework dealumination in zeolite-based SCR catalysts, reducing Brønsted acid site density and ammonia storage capacity (Li et al. 2011; Paolucci et al. 2017). Hydrothermal aging of Fe-zeolite SCR catalysts can induce framework dealumination and transformation of isolated Fe species, leading to decreased NO_X conversion efficiency, particularly at low temperatures where isolated Fe redox sites dominate the reaction pathway (Brandenberger et al. 2008).

Sulphur poisoning occurs through the formation of ammonium sulphates and metal sulphates on active sites, blocking NO_X adsorption and suppressing SCR reaction rates. Ammonium sulphate deactivation is largely reversible and can be regenerated at temperatures above approximately 350 °C, whereas sulphate formation on copper sites may lead to partially irreversible deactivation, especially under repeated sulphur exposure (Hammershøi et al. 2018).

Iron-exchanged zeolite catalysts have attracted growing interest for selective catalytic reduction of NO_X (NH_3-SCR) due to their favourable hydrothermal stability and wide operational temperature window relative to many conventional Cu-exchanged zeolite formulations. Iron-exchanged small-pore zeolites have been demonstrated to maintain significant SCR activity across broad temperature regimes, highlighting their potential for applications requiring robust high-temperature performance (Gao 2020). The catalytic mechanism in Fe-zeolite SCR catalysts relies on redox cycling between Fe^{3+} and Fe^{2+} states, facilitating the oxidation of NO to NO_2 and enhancing the standard SCR reaction pathways (Nasir 2024; Mu 2025). However, Fe-SCR catalysts are also vulnerable to poisoning by phosphorus-containing species, which can accumulate on active sites and block them, leading to a reduction in available active Fe centres and diminished low-

temperature SCR activity (van der Bij and Weckhuysen 2015; Shwan et al. 2014a). Alkali metal (e.g., Na and K) contamination further neutralizes acid sites in Fe-zeolites, decreasing ammonia adsorption capacity and limiting SCR performance (Peng et al. 2020).

Overall, SCR catalyst durability is determined by the combined effects of thermal stress, chemical poisoning, and upstream exhaust composition. Consequently, understanding SCR deactivation, particularly in Fe-SCR systems, is essential for maintaining long-term NO_X reduction efficiency in modern diesel aftertreatment architectures (Nova & Tronconi 2019).

3.4 Catalyst poisons and their effects

In this thesis, the catalysts under investigation were exposed to impurities commonly found in biofuels, including magnesium, potassium, phosphorus, calcium, sodium, and sulphur. This section provides an overview of how these impurities affect SCR and DOC catalysts, with particular emphasis on Fe-based SCR catalysts.

Selective catalytic reduction of NOx with NH_3 relies on the presence of acid sites for ammonia adsorption and redox-active metal centres for NO oxidation. In Fe-zeolite SCR catalysts, isolated Fe^{3+}/Fe^{2+} ions located at ion-exchange sites drive the redox cycle necessary for standard and fast SCR reactions (Shwan et al. 2014b; Gao et al. 2013b). The performance of Fe-SCR catalysts therefore strongly depends on preservation of both zeolite acidity and iron redox chemistry. (Paolucci et al. 2017)

3.4.1 Potassium (K)

Potassium is generally regarded as a poison for SCR catalysts because it neutralises acid sites and suppresses NH_3 adsorption (Lisi & Cimino 2020). In contrast to earlier suggestions, literature indicates that alkali metal (e.g. potassium) addition can alter the acidic and redox properties of Fe-zeolite SCR catalysts. Potassium incorporation affects the distribution and strength of acid sites as well as the redox behaviour of iron species and may in some formulations help to improve alkali resistance compared with conventional oxide supports, resulting in altered catalytic performance. (Putluru et al. 2011.) In Fe-zeolite SCR catalysts, alkali metal species such as K^+ are known to modify

the distribution and coordination environment of iron species. While small amounts may influence the Fe^{3+}/Fe^{2+} redox properties, excessive alkali loading typically neutralises Brønsted acid sites and suppresses catalytic activity, particularly in the fast SCR pathway. (Gao et al. 2013a; Argyle & Bartholomew 2015.)

Alkali metals such as potassium modify zeolite acidity by neutralizing acid sites and altering NH_3 adsorption strength, thereby influencing the interplay between acid and redox functions in NH_3-SCR catalysis (Shwan et al. 2012). While potassium is generally reported to decrease SCR activity at higher loadings due to progressive neutralization of Brønsted acid sites and (in zeolite systems) transport limitations consistent with pore blocking/coverage effects, low alkali concentrations can modify adsorption equilibria and reaction pathways in ways that influence NO_X conversion and product selectivity. The overall effect depends strongly on potassium loading and reaction conditions (Shwan et al. 2015a; Shwan et al. 2015b; Lisi & Cimino 2020). In zeolite systems, potassium exposure has also been linked to increased NO_X storage capacity (formation of new NO_X storage sites), which may contribute to changes in apparent SCR performance under certain conditions (Shwan et al. 2015b).

3.4.2 Phosphorous (P)

Phosphorus is widely recognized as one of the most harmful catalyst poisons. It enters exhaust systems mainly through phosphate-based lubricant additives. In DOC catalysts, phosphorus reacts with platinum and palladium to form thermally stable metal phosphates, which cause severe and largely irreversible loss of oxidation activity. (Kärkkäinen 2017 and references therein).

In SCR catalysts, phosphorus deposits block pores and modify surface acidity by reacting with framework aluminium and active metal species. Phosphorus has been shown to interact with Brønsted acid sites and form stable phosphate species, decreasing acid site density and altering the coordination environment of active metal ions (van der Bij & Weckhuysen 2015; Shwan et al. 2014b). In Fe-zeolite SCR catalysts, phosphorus accumulation near ion-exchange sites can displace iron from active positions and promote dealumination of the zeolite framework, leading to irreversible losses in NO_X conversion efficiency (Shwan et al. 2014b).

3.4.3 Calcium (Ca)

Calcium is less volatile than alkali metals and therefore deposits more slowly on catalyst surfaces. In SCR catalysts, Ca^{2+} can occupy ion-exchange sites and partially neutralize acidity, causing moderate reductions in NH_3 adsorption capacity. (Lisi & Cimino 2020.) In Fe-SCR catalysts, poisoning by alkali and alkaline earth metals can cause chemical deactivation by occupying active sites and reducing acid site density. Among these, calcium induces weaker deactivation than sodium or potassium, but prolonged exposure still leads to reduced NO_X conversion owing to loss of accessible acid and redox sites. (Zhu et al. 2020.) In DOC catalysts, calcium can cover active noble metal sites and reduce oxidation activity, although its impact is typically less severe than that of phosphorus or potassium (Kärkkäinen 2017 and references therein).

3.4.4 Sodium (Na)

Sodium is a well-recognized poison in SCR systems. In vanadium oxide -based SCR catalysts, sodium neutralizes acid sites and reduces surface reducibility, causing significant loss of NO_X conversion (Xiao 2018). In Fe-zeolite SCR catalysts, sodium (Na^+) ions have been shown to compete with Fe^{3+} for ion-exchange positions, thereby decreasing the concentration of isolated iron active sites and lowering redox activity. Alkali metals also modify surface acidity, diminishing Brønsted acid site density and suppressing NH_3 adsorption, which contributes to SCR deactivation (Putluru et al. 2011).

Partial regeneration of sodium-poisoned SCR catalysts by water or mild acid washing has been reported, indicating that Na-induced deactivation can be partly reversible (Xiao 2018). In DOC catalysts, sodium reduces oxidation performance by covering platinum-group metal sites. (Kärkkäinen 2017 and references therein) However, the presence of alkali and alkaline earth metals can lead to irreversible loss of acid sites and structural deterioration, limiting complete recovery of catalytic performance (Zhu et al. 2020).

3.4.5 Sulphur (S)

Sulphur poisoning is a persistent limitation in emission control catalysis (Bartholomew 2001; He et al. 2024). The main mechanisms involve strong chemisorption of sulphur species on active sites, sulfidation of noble or transition metals, and the formation of

stable sulphate deposits that block pores and active centres (Bartholomew 2001; Ma et al. 2022). In diesel oxidation catalysts (DOCs), sulphur compounds can inhibit CO and hydrocarbon oxidation by competitive adsorption on active noble metal sites. Simultaneously, platinum-based formulations promote the oxidation of SO_2 to SO_3, which enhances sulphate formation and may increase particulate mass and sulphur transfer to downstream aftertreatment components. (Russell & Epling 2011.)

Sulphur oxides such as SO_2 and SO_3 (SO_X) are readily formed during combustion and fuel oxidation processes. In SCR systems, SO_3 especially has a pronounced tendency to form sulphates, including ammonium sulphate and bisulphate, which contribute to particulate formation and can block active catalytic sites. These sulphate species have been shown to interact strongly with catalyst surfaces, leading to loss of NO_X reduction activity and accelerated deactivation. (Cheng et al. 2010) Deposited metal sulphates formed during SO_2 exposure are thermally stable under typical diesel exhaust temperatures, making complete regeneration challenging and leading to progressive long-term deactivation (Forzatti 2001; Brandenberger et al. 2008).

In zeolite-based SCR systems such as Cu-SSZ-13 and Fe-zeolites, sulphur poisoning affects ion-exchange sites, modifies the Cu redox cycle, and promotes the formation of ammonium sulphate species at low temperatures, resulting in decreased NO_X conversion efficiency (Gao et al. 2013a; Jiang et al. 2016). Within Fe-based SCR catalysts, sulphur species preferentially interact with redox-active Fe^{3+}/Fe^{2+} centres associated with the zeolite framework, and the formation of sulphate species on these sites has been identified as a key cause of suppressed redox cycling. Such suppression inhibits the standard SCR reaction mechanism that relies on efficient Fe^{3+}/Fe^{2+} interconversion for catalytic activity. (Zhao et al. 2022.) Fe-zeolite catalysts generally exhibit higher intrinsic sulphur tolerance than Cu-zeolites due to differences in sulphate formation pathways and redox chemistry. However, prolonged SO_2 exposure still results in gradual deactivation associated with the formation of thermodynamically stable iron sulphate species such as $Fe_2(SO_4)_3$, which block active redox sites and suppress Fe^{3+}/Fe^{2+} cycling. (Gao 2020.) Low-temperature operation promotes the formation of ammonium bisulphate, which deposits inside catalyst pores and causes severe but partially reversible deactivation in NH_3-SCR systems (Li et al. 2017; Guo et al. 2021).

Sulphur species adsorb strongly on Pt and Pd surfaces, forming stable sulphates that block active sites and inhibit oxidation reactions (Shelef & McCabe 2000; Russell & Epling 2011). In addition, sulphur interacts with ceria–zirconia oxygen storage materials, decreasing oxygen storage capacity (OSC) and impairing air–fuel ratio buffering (Kim et al. 2022). While desulphation treatments at elevated temperatures can partially restore performance, repeated sulphur exposure accelerates long-term catalyst degradation (Kim et al. 2022).

Mitigation strategies include improved catalyst formulations using sulphur-tolerant supports or promoters, operational optimization to limit sulphate stability, and regeneration by oxidative or thermal methods (Lambert 2004; He et al. 2024; Lee et al. 2024). To mitigate sulphur poisoning and enhance durability, several strategies have been investigated for Fe-SCR systems. These include optimization of framework composition to improve hydrothermal stability, incorporation of promoter elements that modify sulphate binding strength, and regeneration protocols combining high-temperature oxidative treatments with controlled steam exposure to remove sulphate deposits and partially restore isolated Fe sites (Gao 2020; Chen et al. 2022; Zhao et al. 2022). Nevertheless, the most reliable protection remains the use of low-sulphur fuels (Lambert 2004; Xie et al. 2020). Although surface sulfation may be partially reversible at elevated temperatures, repeated sulphur exposure–regeneration cycles often result in gradual structural degradation, including dealumination and irreversible redistribution of iron species (Brandenberger et al. 2008; Chen et al. 2022).

3.5 Catalyst regeneration

Catalyst regeneration refers to the restoration of catalytic performance after activity loss during operation (Argyle & Bartholomew 2015). In NH_3-SCR exhaust aftertreatment systems, regeneration aims to recover NO_X conversion efficiency while avoiding additional thermal or structural damage to the catalyst (Nova and Tronconi 2014). In mobile and stationary applications, regeneration may be performed in situ through controlled exhaust temperature management or ex situ via industrial reconditioning processes, particularly in large stationary SCR units (Zhao et al. 2024). The feasibility and degree of recovery depend strongly on catalyst formulation, particularly for V_2O_5–

WO_3/TiO_2 and Fe-zeolite SCR catalysts, whose structural characteristics govern regeneration behaviour (Li et al. 2011; Colombo et al. 2010).

3.5.1 Thermal regeneration

Thermal treatment is the primary regeneration strategy for SCR catalysts affected by reversible surface deposits (Ma et al. 2022). In V_2O_5–WO_3/TiO_2 catalysts, elevated temperatures between 600–700 °C promote decomposition of surface sulphate species and ammonium salts, enabling partial restoration of vanadia redox functionality (Busca et al. 1998; Song et al. 2021). Industrial practice in stationary SCR units frequently applies controlled high-temperature operation periods to remove surface sulphates accumulated during low-temperature operation (Nova and Tronconi 2014). However, regeneration temperature must be carefully controlled, as excessive temperatures can induce vanadia sintering and support phase transformation above 600 °C, thereby reducing long-term durability even if short-term activity improves (Busca et al. 1998; Nova and Tronconi 2014). Consequently, optimized thermal protocols seek to balance sulphate decomposition with minimal structural alteration (Ma et al. 2022).

For Fe-zeolite SCR catalysts such as Fe-ZSM-5, thermal regeneration can remove ammonium sulphate deposits and certain iron sulphate species formed during operation (Colombo et al. 2010). Oxidative treatment below 600 °C has been shown to restore NH_3 adsorption capacity and partially recover NO_X conversion when regeneration targets surface-bound species (Ma et al. 2022; Shen et al. 2019). Nevertheless, regeneration efficiency decreases if structural alterations accompany contaminant accumulation, as thermal treatment cannot reconstruct zeolite framework integrity or reverse metal redistribution within the framework (Li et al. 2011; van der Bij & Weckhuysen 2015). The mobility of exchanged metal ions during heating influences active site reformation, making controlled oxidative environment preferable to avoid excessive metal migration (Colombo et al. 2010).

3.5.2 Chemical regeneration

Chemical regeneration in SCR exhaust aftertreatment refers to restoration strategies that rely on reactive gas environments or solution-based treatments to remove contaminants, re-establish active surface chemistry, or recondition catalyst composition (Nova and

Tronconi 2014; Argyle & Bartholomew 2015). In stationary SCR systems, chemical regeneration is typically performed ex situ, whereas mobile applications rely primarily on in situ gas-phase treatments due to system constraints (Nova and Tronconi 2014; Zhao et al. 2024).

For V_2O_5–WO_3/TiO_2 SCR catalysts, chemical regeneration may combine removal of surface contaminants with partial restoration of vanadia functionality (Ma et al. 2022). Oxidative–reductive treatments can facilitate decomposition of surface-bound species and re-establish vanadium redox cycling when the catalyst structure remains intact (Busca et al. 1998; Song et al. 2021). In industrial stationary applications, chemical reconditioning may also include re-impregnation with vanadium precursors followed by calcination, enabling recovery of NO_X conversion efficiency through replenishment of active surface species (Qi et al. 2017; Qian et al. 2022a).

Within this framework, acid washing represents a targeted ex situ treatment primarily investigated for V-based SCR catalysts (Cao et al. 2019; Qian et al. 2022a). Mineral acids such as HNO_3 and H_2SO4, as well as organic acids such as oxalic acid, can dissolve deposited alkali and alkaline earth species and increase accessibility of catalytically active sites, leading to measurable recovery of SCR activity when structural integrity is preserved (Cao et al. 2019; Zhao et al. 2024). However, acid leaching may also modify vanadium dispersion or partially extract active components, which can influence long-term durability (Qian et al. 2022a). Consequently, acid washing is often integrated with controlled re-impregnation and calcination rather than used as an independent regeneration method (Qi et al. 2017).

For Fe-zeolite SCR catalysts, chemical regeneration must preserve the aluminosilicate framework, since catalytic performance depends directly on framework acidity and the coordination environment of exchanged Fe species (Li et al. 2011; Colombo et al. 2010). Strong acid treatments can induce dealumination and modify Brønsted acid sites, thereby affecting NH_3 adsorption and SCR reaction pathways (Velichkina et al. 2021; Lisi & Cimino 2020). Consequently, acid-based regeneration is generally considered unsuitable for practical Fe-SCR exhaust systems, where preservation of framework integrity is essential (Nova and Tronconi 2014). Instead, regeneration of Fe-SCR catalysts relies mainly on controlled gas-phase treatments designed to restore surface chemistry without compromising structural stability (Ma et al. 2022).

Overall, chemical regeneration of SCR catalysts, whether through reactive gas treatments, acid washing, or re-impregnation, can provide partial restoration of catalytic performance when surface contamination dominates, but it cannot reconstruct the original catalyst architecture if structural integrity has been altered (Qian et al. 2022b; Li et al. 2011). Although reversible surface contamination can often be mitigated through thermal or chemical treatments, repeated aging–regeneration sequences generally result in gradual loss of accessible active sites and declining NO_X conversion efficiency (Paolucci et al. 2017; Qian et al. 2022b).

3.5.3 Regeneration in practical exhaust systems

In practical exhaust aftertreatment, regeneration strategies are integrated into system-level control to maintain SCR performance under varying operation conditions (Nova and Tronconi 2014). In stationary SCR reactors, periodic high-temperature operation is applied to remove sulphate deposits accumulated during prolonged low-load or low-temperature operation. (Nova and Tronconi 2014; Zhao et al. 2024). Such operational regeneration is typically implemented during planned maintenance intervals or controlled load increases in power plant applications (Zhao et al. 2024). In mobile diesel applications, exhaust temperature management through engine calibration strategies, late fuel injection, or auxiliary heating systems can induce desulfation events under controlled conditions. However, temperature excursions must be carefully managed to avoid accelerated catalyst aging or structural degradation. (Nova and Tronconi 2014.)

The long-term effectiveness of regeneration depends on minimizing cumulative structural degradation during repeated thermal cycles (Ma et al. 2022). Although reversible surface contamination can often be mitigated through thermal or chemical treatments, repeated aging-regeneration sequences generally result in gradual loss of accessible active sites and declining NO_X conversion efficiency (Paolucci et al. 2017; Qian et al. 2022b). Consequently, regeneration in SCR aftertreatment systems is regarded primarily as a lifetime-extension strategy rather than a complete restoration of original catalyst performance (Li et al. 2011; Nova and Tronconi 2014).

3.6 Deactivation in perspective of economic and environmental sustainability

Sustainability refers to the responsible use of existing resources to meet the needs of the present generation without compromising the ability of future generations to meet their own needs. This definition originates from the Brundtland Report, published by the World Commission on Environment and Development in 1987. (World Commission on Environment and Development 1987). More recent sustainability research emphasizes operational resource efficiency and circular material flows as key industrial strategies for achieving this goal (Geissdoerfer et al. 2017; Kirchherr et al. 2017). Within industrial contexts, sustainability requires a critical evaluation of energy and material consumption. While sustainability encompasses multiple dimensions, including environmental, economic, social, and cultural factors, this work focuses specifically on the environmental and economic aspects. In process industries, environmental and economic sustainability are closely linked, as energy and material inefficiencies directly translate into both emissions and financial losses (IEA 2022; Pinciroli et al. 2023). In practice, maintenance strategy and reliability strongly influence resource efficiency because failures and corrective actions generate additional energy use, material consumption and emissions across the asset lifecycle (Pinciroli et al. 2023).

From an environmental perspective, sustainable use of chemicals and energy is essential. This aligns with the principles of green chemistry, which emphasize waste prevention, energy efficiency, and the design of safer chemicals and processes (Anastas & Warner 1998). Catalysis is widely recognised as a cornerstone of sustainable chemical manufacturing: catalytic processes are estimated to be involved in the manufacture of up to ca. 90% of all commercially produced chemical products, demonstrating their immense role in process efficiency and material transformations (Hughes 2021; Schlögl 2015). These catalyst-enabled processes contribute significantly to reducing energy demand, improving selectivity, and lowering waste generation in comparison with non-catalysed processes (Sheldon & Brady 2018). One of the key environmental challenges in catalysis is catalyst deactivation. When a catalyst loses activity and cannot be regenerated and reused, it effectively becomes industrial waste. This not only results in the loss of valuable materials and the energy used to produce them but also introduces additional waste management issues. (Bartholomew 2001; Al-Zubaidi & Yang 2020). Globally, the

chemical industry generates over 300 million tonnes of solid waste annually, and spent catalysts represent a significant fraction of hazardous industrial waste streams (OECD 2019; Bobba et al. 2020). In addition, the production of many heterogeneous catalysts involves critical raw materials such as platinum-group metals, whose extraction is energy-intensive and associated with substantial environmental burdens (Habib & Wenzel 2016; Bobba et al. 2020; Hughes 2021; Kamran et al. 2023). For example, automotive catalytic converters contain small but significant amounts of PGMs, typically in the range of 3–7 g of Pt, 1.5–5 g of Pd and 0.8–1.5 g of Rh per catalyst unit, and demand for these metals is heavily driven by catalyst use (Yakoumis 2023). The extraction of PGMs from primary ores is energy-intensive and environmentally impactful, which further elevates the importance of recycling and recovery (Kamran et al. 2023). Recycling technologies can recover up to ~95% of the PGMs contained in spent automotive catalysts, and recycling one tonne of used converters can avoid the need to extract many tonnes of primary ore and associated waste rock (Yakoumis 2023). Despite this potential, the recycling rate of spent catalysts remains suboptimal in many regions, resulting in loss of valuable resources and continued demand for primary mining (Xia et al. 2023).

Selective catalytic reduction (SCR) is a key technology for reducing NO_X emissions from lean-burn and diesel engines. Iron-exchanged zeolite catalysts (Fe-SCR) are attractive from environmental and economic sustainability perspectives because iron is abundant, inexpensive, and less supply-critical than noble metals (Liu et al. 2020). In addition to these resource advantages, Fe-zeolite catalysts operate over a relatively wide temperature window and exhibit good resistance to hydrothermal degradation, supporting long-term durability under demanding automotive conditions (Brandenberger et al. 2008; Liu et al. 2020). Together, these characteristics reduce dependence on critical raw materials and contribute to the lifecycle sustainability of Fe-based SCR systems. However, Fe-exchanged zeolite catalysts remain susceptible to deactivation mechanisms, particularly hydrothermal ageing, framework dealumination and changes in the coordination environment of Fe species under prolonged high-temperature exposure, which progressively diminish catalytic performance during long-term operation (Gao et al. 2013a).

Economically, catalysts often represent a major financial investment, particularly in industries such as petrochemicals, pharmaceuticals and energy. When a catalyst deactivates, the original investment is lost, and new costs arise from replacement and

waste management. Regeneration can reduce some of these costs, but it still requires inputs in the form of energy, chemicals and labour. (Thomas & Thomas 2015.) Moreover, frequent regeneration or replacement can lead to operational downtime, which introduces further inefficiencies. From this perspective, too, the development of long-lasting catalysts offers a clear advantage. In a comparative economic analysis of catalytic processes, sustained catalyst activity (longer catalyst lifetime before replacement) was found to dramatically reduce total manufacturing costs. Specifically, costs decreased systematically with higher catalyst activity maintenance, leading to total manufacturing cost reductions of between approximately 37% and 75% in continuous processes relative to cases with short catalyst life or frequent catalyst change-out events. (Mendoza et al. 2025.) Furthermore, noble-metal-based catalysts may account for up to 20–40% of the total capital cost of certain chemical reactor systems, highlighting the strong economic incentive for extending catalyst lifetime (Sheldon & Brady 2018; Bobba et al. 2020).

In summary, promoting sustainability in industrial catalysis involves more than just managing waste or recycling materials. It requires a shift toward the design of catalysts that are inherently more stable and efficient. While regeneration remains a useful tool, it should be seen as a secondary solution rather than the primary goal. Focusing research efforts on improving catalyst durability has the potential to reduce environmental impact and operating costs alike, making it rational and forward-looking strategy for sustainable industrial processes. Quantitatively, improving catalyst lifetime by only 20–30% has been estimated to reduce lifecycle greenhouse gas emissions of catalytic reactor systems by 10–25%, primarily through avoided replacement production and waste treatment (Bobba et al. 2020). These figures illustrate that catalyst durability is not only a technical objective but also a measurable sustainability lever.

4 METHODS AND MATERIALS

4.1 Experimental work – exposure of catalysts to impurities

The catalysts investigated in this work were subjected to controlled ageing treatments in order to evaluate their resistance to deactivation by typical exhaust-gas impurities. The samples consisted of honeycomb-structured monolithic catalysts cut from a larger monolith (400 cells per in^2, cpsi). Each specimen had a diameter of 9 mm and a length of 35 mm, corresponding to a catalyst volume of approximately 2.23 cm^3. The samples were placed in a quartz tubular reactor and supported from below with quartz wool to ensure stable positioning during thermal treatment. The main geometric parameters of the catalyst samples and calculated flow-related quantities, including gas hourly space velocity (GHSV), are summarised in Table 1.

Table 1. Flow and reactor operating parameters.

Parameter	Value	Unit	Notes
Catalyst shape	Cylindrical monolith	-	Honeycomb structure
Catalyst diameter	0.9	cm	
Catalyst length	3.5	cm	
Catalyst volume	2.23	cm^3	Calculated
Total gas flow	1000	mL/min	Incl. vapour
Total gas flow	60 000	mL/min	Converted
GHSV	2.7×10^4	h^{-1}	Calculated
Liquid feed rate	0.26	mL/min	Water or impurity solution
Ageing temperature	500	°C	
Ageing duration	5	h	

The quartz reactor was installed inside a tubular furnace equipped with temperature control. Gas flows were regulated using mass flow controllers. The total gas flow rate during ageing experiments was maintained at 1000 mL/min, corresponding to a gas hourly space velocity (GHSV) of approximately 2.7×10^4 h^{-1}.

During ageing, a synthetic gas mixture consisting of nitrogen, oxygen and sulphur dioxide was supplied to the reactor. The composition of the ageing gas mixture is presented in Table 2. Nitrogen served as the balance gas, oxygen was introduced to simulate oxidising exhaust conditions, and sulphur dioxide was supplied from a certified gas cylinder to achieve a concentration of 100 ppm in the feed gas. The reactor equipment is presented in Figure 1.

Table 2. Gas mixture composition during ageing.

Element	Concentration	Unit	Notes
N_2	70	vol-%	Balance gas
O_2	10	vol-%	Oxidising component
SO_2	100	ppm	Sulphur poisoning
H_2O	from 0.26 mL/min feed	-	Evaporated in reactor
Impurity compound (K/Na/Ca/P)	from 0.1 M solution	-	Present only during poisoning experiments

Figure 1. Ageing equipment.

Water was introduced into the reactor by continuously feeding an aqueous solution at a rate of 0.26 mL/min using a peristaltic pump. The liquid feed evaporated inside the heated reactor, generating water vapour in the gas stream.

For impurity poisoning experiments, aqueous metal salt solutions (Na, K, Ca or P; 0.1 M) were fed in the same manner at the liquid flow rate of 0.26 mL/min. The solution droplets vaporised upon entering the hot reactor, forming an aerosol that transported the impurity species to the catalyst surface. The preparation of the impurity solutions and feeding conditions are listed in Table 3.

Table 3. Impurity solution preparation and feeding conditions.

Element	Salt used	Salt amount (g)	Water (mL)	Solution molarity (M)	Liquid feed rate (mL/min)
Na^{+}	$NaNO_3$	0.217	100	0.1	0.26
K^{+}	KNO_3	0.063	100	0.1	0.26
Ca^{+2}	$Ca(NO_3)_2$	0.178	100	0.1	0.26
P^{+5}	H_3PO_4	0.102	100	0.1	0.26

All ageing experiments were conducted at 500 °C for a total duration of five hours. The ageing experiments were carried out ex-situ in a reactor different from the one used for activity measurements. Prior to ageing, the reactor was heated to the target temperature under a nitrogen–oxygen gas mixture. Once the desired temperature was reached, the ageing gas mixture containing N_2, O_2, SO_2 and water-impurity solution was introduced. For impurity poisoning experiments, the metal salt solution feed was started simultaneously with the SO_2 supply. After completion of the five-hour ageing period, the impurity and SO_2 feeds were stopped and the reactor was cooled to room temperature under a continuous nitrogen flow to prevent uncontrolled oxidation of the catalyst surface.

The applied ageing conditions included hydrothermal ageing alone, hydrothermal ageing in the presence of sulphur, and combined ageing with sulphur and individual impurity elements (Na, K, Ca or P) in the presence of water. The experimental matrix is summarised in Table 4. All ageing procedures were carried out on Fe-SCR catalysts in order to evaluate their resistance to deactivation under different poisoning environments.

Table 4. Ageing experiment matrix for Fe-SCR catalysts.

Experiment type	SO_2	H_2O	Na	K	Ca	P
Hydrothermal ageing	-	x	-	-	-	-
Hydrothermal + sulphur	x	x	-	-	-	-
Sulphur + Na poisoning	x	x	x	-	-	-
Sulphur + K poisoning	x	x	-	x	-	-
Sulphur + Ca poisoning	x	x	-	-	x	-
Sulphur + P poisoning	x	x	-	-	-	x

4.2 Activity measurements

Following the ageing treatments, the catalytic activity of the poisoned Fe-SCR samples was evaluated in dedicated activity tests. Each catalyst sample was placed inside a quartz reactor tube and supported by quartz wool at the bottom of the reactor to maintain a fixed position and uniform gas flow. A schematic illustration of the activity measurement setup is shown in Figure 2.

Figure 2. Activity measurement equipment.

The catalyst dimensions were identical to those used in the ageing experiments (diameter 9 mm, length 35 mm), corresponding to a catalyst volume of approximately 2.23 cm^3. The total gas flow rate during activity measurements was 1500 mL/min, which corresponds to a gas hourly space velocity (GHSV) of approximately 4.0×10^4 h^{-1}. The main flow parameters are summarised in Table 5.

Table 5. Flow and operating parameters during activity measurements.

Parameter	Value	Unit	Notes
Catalyst volume	2.23	cm^3	Cylindrical monolith
Total gas flow	1500	mL/min	Including vapour
GHSV	4.0×10^4	h^{-1}	
Reactor temperature	up to 550	°C	
Heating rate	10	°C/min	
Catalyst placement	Quartz tube reactor	-	Supported by quartz wool
Gas analysis	Gasmet™ analyser	-	Continuous monitoring

During activity testing, the samples were exposed to a synthetic gas mixture simulating SCR reaction conditions. The feed gas consisted of 8 vol-% H_2O (steam), 7 vol-% O_2, 500 ppm NO, 400 ppm NH_3, and 70 ppm N_2O, with nitrogen serving as the balance gas. Water was introduced through a liquid feed system, vaporised in a preheater, and supplied to the reactor as steam. Gas flow rates were regulated using mass flow controllers to ensure stable and reproducible feed conditions. The detailed gas mixture composition is listed in Table 6.

Table 6. Gas mixture composition during activity measurements.

Gas component	Concentration	Unit	Notes
H_2O	8	%	From vaporised liquid feed
O_2	7	%	
NO	500	ppm	
NH_3	400	ppm	
N_2O	70	ppm	
N_2	balance	-	Carrier gas

The reactor temperature was ramped to 550 °C at a heating rate of 10 °C min^{-1} during the activity measurements. The concentrations of inlet and outlet gas components were continuously monitored using a Gasmet™ gas analysis system. This setup enabled

continuous observation of catalytic performance as a function of temperature, providing information on the activity of the aged catalysts under simulated SCR reaction conditions.

4.3 Characterization methods

4.3.1 Specific Surface Area (BET)

The Brunauer–Emmett–Teller (BET) method is a widely applied technique for determining the specific surface area of porous and nanostructured materials based on multilayer adsorption theory. Nitrogen physisorption at liquid nitrogen temperatures enables quantification of surface area, pore volume and, through Barrett–Joyner–Halenda (BJH) analysis, the mesopore size distribution. (Gregg & Sing 1982) For catalytic materials, BET analysis provides essential insight into how surface area and porosity influence the accessibility of active sites, diffusion properties, and support–active phase interactions (Thommes et al. 2015). Recent developments in adsorption theory, standardized physisorption methodologies and high-resolution isotherm analysis have significantly improved the reliability of surface area and pore size determination in micro and mesoporous as well as hierarchically structured materials. In this context, BET analysis remains a fundamental and widely applied method for the characterization of catalysts, adsorbents and metal oxide supports when used according to established consistency criteria and in combination with advanced models such as density functional theory (Thommes et al. 2015; Schlumberger and Thommes 2021).

4.3.2 Diffuse Reflectance Infrared Fourier Transform Spectroscopy

Diffuse Reflectance Infrared Fourier Transform Spectroscopy (DRIFTS) is a powerful vibrational technique for probing surface species, adsorbates and reaction intermediates on heterogeneous catalysts under operando or in situ conditions. Owing to its sensitivity to surface functional groups and acid–base sites, DRIFTS is particularly suited for investigating adsorption and desorption phenomena on powdered and porous solid catalysts, such as metal oxides, zeolites, and supported materials (Shi et al. 2020). The technique enables identification of Brønsted and Lewis acid sites, monitoring of redox cycles, and elucidation of reaction pathways by tracking real-time changes in surface-bound species under reaction conditions (Montanari et al. 2007).

4.3.3 X-ray Diffraction

X-ray diffraction (XRD) is a fundamental technique for determining crystal structure, phase composition, crystallite size and structural stability of catalyst materials. Based on Bragg's law, XRD patterns reveal the long-range order of crystalline phases, enabling identification of active oxides, supports, dopants and any phase transformations during synthesis or operation. (Cullity & Stock 2014.) In heterogeneous catalysis, XRD is widely used to evaluate dispersion of metal nanoparticles, detect amorphous versus crystalline contributions, and monitor structural evolution during thermal treatment or reaction cycling (Bulavchenko & Vinokurov 2023).

4.3.4 Scanning Electron Microscopy

Scanning Electron Microscopy (SEM) provides high-resolution imaging of catalyst morphology, particle size, surface texture and the spatial distribution of active phases. By scanning a focused electron beam across the surface, SEM produces secondary and backscattered electron signals that reveal topographical and compositional contrast at nanometre–micrometre scales. (Goldstein et al. 2018) For catalytic materials, scanning electron microscopy (SEM) is essential for assessing catalyst morphology, particle agglomeration and dispersion, as well as structural changes following ageing or hydrothermal treatment; when coupled with energy-dispersive X-ray spectroscopy (EDS) it enables simultaneous morphological imaging and semi-quantitative elemental mapping, facilitating correlations between surface structure and catalytic behaviour (Chee et al. 2023).

5 RESULTS AND DISCUSSION

5.1 Activity measurements

As a baseline, a blank experiment was performed using an empty reactor setup without a catalyst sample to verify that no significant NOx conversion occurs in the absence of catalytic material. The measured gas concentrations during the temperature ramp showed stable NO and NH_3 levels throughout the experiment, while NO_2 remained close to zero. No decrease in NO concentration attributable to catalytic activity was observed. This confirms that gas-phase reactions or reactor wall effects did not contribute measurably to NO_X conversion under the applied test conditions. Therefore, any NO_X removal detected in subsequent experiments can be attributed to catalytic activity rather than system artefacts. The experimental data is presented in detail in the Appendix 1. In Figure 3 is presented an example of activity measurement over poisoned sample.

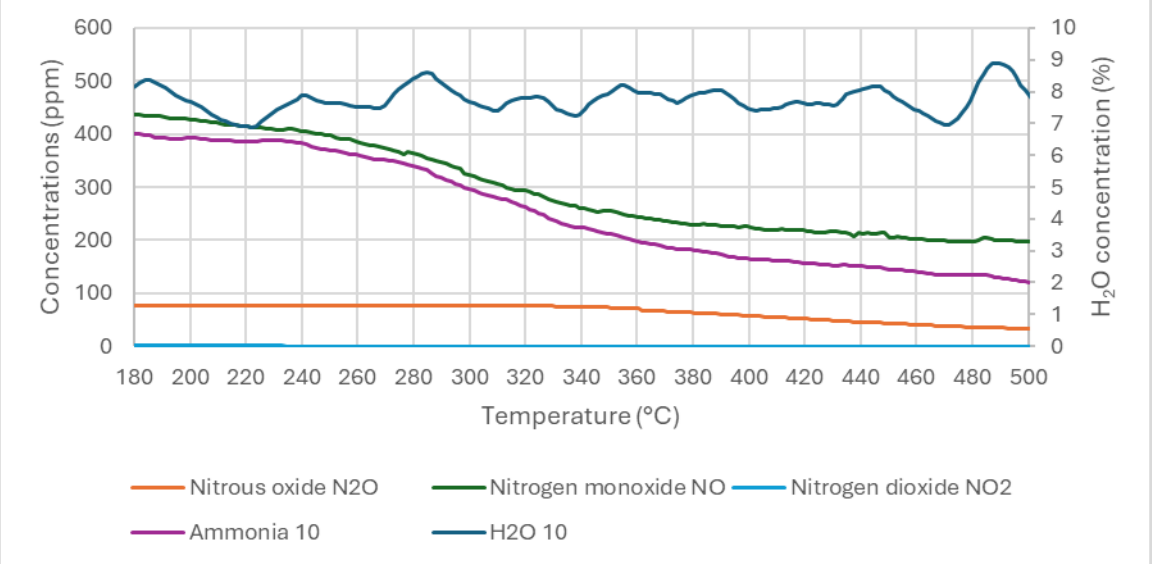

Figure 3. Example of activity measurement over CaSHT poisoned Fe-SCR catalyst.

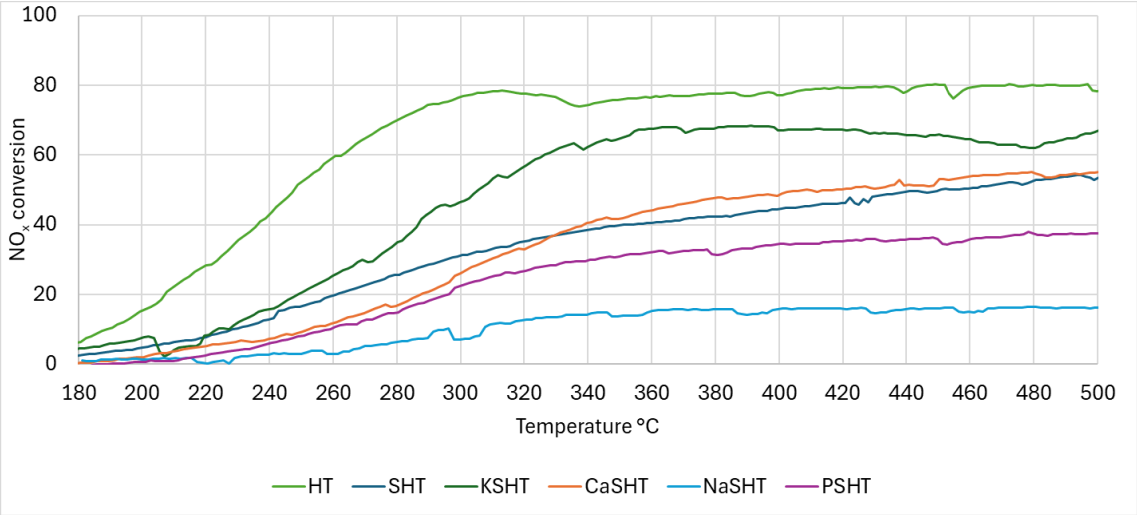

Figure 4. NO_X conversions by deactivation conditions.

In Figure 4 the NO_X conversions over deactivated catalysts are presented. The maximum possible NO_X conversion in SCR experiments was 80 % by the feed gas with NH_3/NO_X = 0.8. It was seen that the effect of chemical poisoning by K, Na, Ca and P was very heavy, when significant drops in SCR activity was seen with all samples in comparison to SHT aged sample. For the Fe–SCR catalyst aged in the presence of sulphur, potassium, and water (KSHT), NO_X conversion initiated at approximately 220–240 °C, indicating an early onset of SCR activity. Conversion increased rapidly with temperature and reached approximately 67 % at 500 °C, forming the highest conversion plateau among all sulphur-aged samples. The relatively low light-off temperature combined with the high plateau conversion demonstrates that potassium addition partially restores SCR activity after sulphur ageing. This behaviour suggests that potassium modifies surface acidity, active sites and/or redistributes sulphur species in a manner that preserves accessible iron redox sites and promotes NH_3–NO_X reaction kinetics. Alkali metals are reported to alter zeolite acidity and influence sulphate stability on Fe–zeolites (Brandenberger et al. 2008; Liu et al. 2020).

For the Fe–SCR catalyst aged in the presence of sulphur, calcium, and water (CaSHT), NO_X conversion began at approximately 240–260 °C and increased steadily to a maximum of approximately 55 % at 500 °C. The conversion profile lies consistently above that of the sulphur-only aged sample (SHT), demonstrating that calcium addition also enhances retained SCR activity after sulphur exposure. However, the conversion plateau remains significantly lower than that of the potassium-modified sample, indicating that calcium only partially mitigates sulphur-induced deactivation. This

suggests that calcium induces moderate modification of adsorption and redox properties but does not restore full accessibility of iron active sites. Interactions between alkaline earth metals and surface sulphates have been discussed in Fe-zeolite deactivation studies (Liu et al. 2020).

When the Fe–SCR catalyst was aged with sulphur, sodium, and water (NaSHT), NO_X conversion remained negligible below approximately 300 °C and increased only slightly at higher temperatures, reaching merely ~16 % at 500 °C. The absence of substantial conversion throughout the ramp indicates severe deactivation of SCR functionality. The strongly suppressed profile suggests that sodium neutralizes surface acidity and disrupts iron active sites, preventing efficient NH_3 adsorption and NO_X reduction. Among all examined poisons, sodium therefore produces the most pronounced loss of SCR performance. Neutralisation of Brønsted acid sites by alkali metals and the associated loss of SCR activity are well documented (Brandenberger et al. 2008; Liu et al. 2020).

In the presence of sulphur, phosphorus, and water (PSHT), NO_X conversion initiated at approximately 260–280 °C and increased gradually with temperature, reaching as low maximum as ~38 % at 500 °C. The absence of a clear high-conversion plateau indicates persistent limitation in SCR reaction rates across the temperature range. Compared with SHT and CaSHT, phosphorus clearly suppressed retained SCR activity, demonstrating that phosphate formation blocks a significant fraction of iron sites and adsorption centres. This behaviour is consistent with strong chemical poisoning rather than reversible surface modification. Formation of stable metal phosphate species and their inhibitory effect on SCR catalysts have been reported in recent studies (Liu et al. 2020; Park 2024).

For the Fe–SCR catalyst subjected only to hydrothermal ageing without additional chemical poisons (HT), NO_X conversion initiated at approximately 230–250 °C and increased steadily with temperature, reaching approximately 60–65 % at 500 °C. Hydrothermal ageing of Fe–zeolite catalysts is known to induce dealumination and partial migration or aggregation of Fe species, leading to reduced Brønsted acidity but not complete loss of redox functionality (Brandenberger et al. 2008; Liu et al. 2020). Recent investigations further demonstrate that although steaming alters Fe coordination environments, a significant fraction of isolated Fe active sites remains accessible after hydrothermal treatment (Buttignol et al. 2022; Park 2024). The retained conversion level

observed here is therefore consistent with structural ageing rather than severe chemical poisoning.

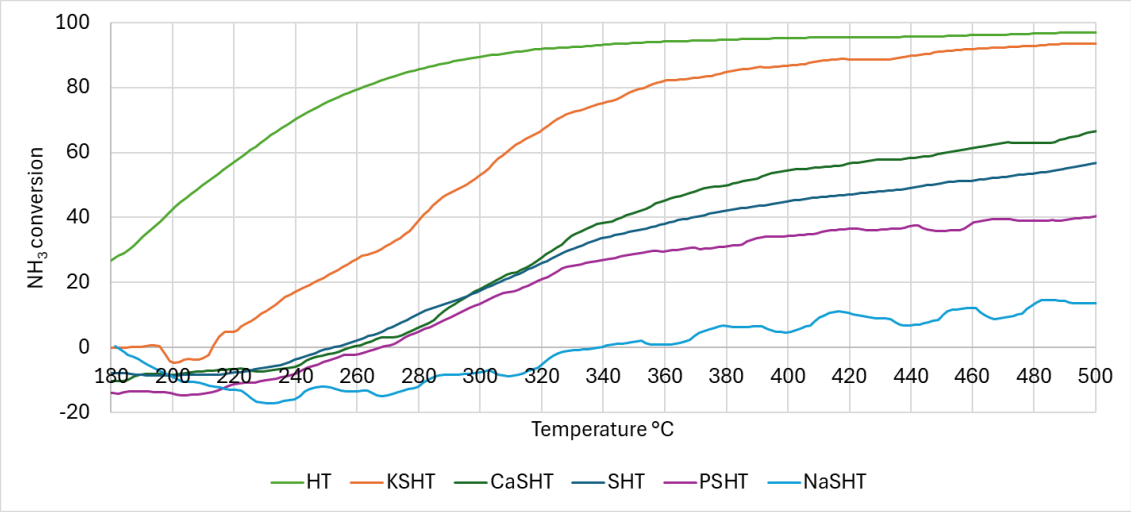

Figure 5. NH_3 conversions by deactivation conditions.

In general, NH_3 conversions (Figure 5) correlate well to NO_X conversions by the consumption in SCR reaction (NO + NH_3). However, the poisons had significant poisoning effect also on NH3 oxidation in comparison to the HT aged sample. NH_3 conversion over KSHT initiated already at approximately 200–220 °C, demonstrating facile NH_3 adsorption and activation. Conversion increased steeply with temperature and reached approximately 95% at 500 °C, forming a near-complete conversion plateau. This high NH_3 conversion indicates that potassium decreased less than other poisons NH_3 adsorption. The discrepancy between very high NH_3 conversion and only moderate NO_X conversion suggests that downstream redox steps or nitrogen recombination remain partially limited. Effects of alkali metals on ammonia storage and SCR kinetics are discussed in detail by Liu et al. (2020).

For CaSHT, NH_3 conversion began at approximately 240–260 °C and increased steadily to approximately 67% at 500 °C. The moderate conversion plateau indicates partial preservation of NH_3 adsorption and activation capacity after Ca–S ageing. Compared with SHT, calcium improves NH_3 conversion, but the incomplete plateau confirms that a fraction of adsorption or redox sites remains blocked. Partial retention of ammonia adsorption capacity after alkaline earth modification has been reported in Fe-SCR systems (Liu et al. 2020).

For NaSHT, NH_3 conversion remained close to zero below approximately 300 °C and reached only ~14% at 500 °C. The nearly flat conversion curve demonstrates that sodium severely inhibits NH_3 adsorption and activation. This behaviour is consistent with strong neutralization of surface acid sites and disruption of SCR-relevant adsorption equilibria. Alkali-induced suppression of NH_3 adsorption in zeolite catalysts is widely reported (Brandenberger et al. 2008; Liu et al. 2020).

For PSHT, NH_3 conversion started near 260 °C and increased gradually to approximately 40% at 500 °C. The relatively low plateau indicates strong suppression of NH_3 adsorption and/or activation. Phosphate formation likely blocks adsorption sites and immobilizes neighbouring iron redox centres, limiting the number of catalytically competent sites. Consequently, NH_3 activation remains incomplete even at high temperature. Phosphorus poisoning mechanisms in SCR catalysts have been reviewed recently (Park 2024).

For the HT sample, NH3 conversion began at approximately 220–240 °C and increased to approximately 85–90% at 500 °C. Although hydrothermal ageing reduces acid site density through framework dealumination (Brandenberger et al. 2008), spectroscopic studies indicate that residual Brønsted and Lewis acid sites remain available for NH_3 adsorption even after severe steaming (Buttignol et al. 2022). The relatively high NH_3 conversion observed here therefore suggests that ammonia availability is not the primary limiting factor for the HT catalyst.

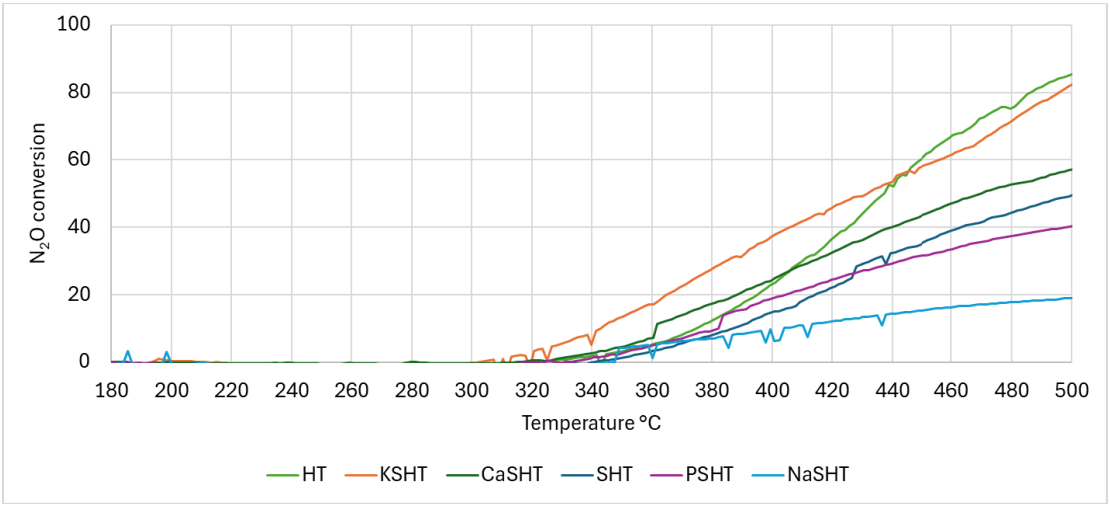

Figure 6. N_2O conversions by deactivation conditions.

The studied Fe-Beta is known to show activity also for N_2O decomposition. Therefore, we received information also about the effect of these poisons in N_2O reactions (decomposition and reduction by NH_3). The lowest light-off (T_{50}) in N_2O removal (Figure 6) was about 440 °C, which is quite typical for Fe-zeolites. N_2O conversion over KSHT initiated at approximately 320–330 °C and increased continuously to approximately 82% at 500 °C. This represents the highest retained N_2O decomposition activity among all sulphur-aged samples. The relatively early onset and high plateau indicate that potassium addition preserves or partially restores redox-active iron sites and oxygen vacancy formation capacity required for N–O bond cleavage. Nevertheless, the elevated light-off temperature compared with fresh catalysts indicates that sulphur poisoning is not fully eliminated. The role of Fe^{3+}/Fe^{2+} redox cycling in N_2O decomposition over Fe-zeolites has been discussed in mechanistic studies (Zhang et al. 2018).

For CaSHT, N_2O conversion began at approximately 340–350 °C and increased steadily to approximately 57% at 500 °C. The conversion curve lies above that of the sulphur-only aged sample, indicating improved redox functionality relative to SHT. However, the moderate plateau demonstrates that only partial recovery of N_2O decomposition activity occurs after Ca addition. Redox-site preservation after alkaline earth modification has been reported in Fe-SCR literature (Liu et al. 2020).

For PSHT, N_2O conversion initiated near 360 °C and reached only ~40% at 500 °C. The uniformly low conversion indicates strong suppression of redox cycling and oxygen vacancy formation. The formation of stable phosphate phases likely immobilizes iron centres essential for N_2O activation, resulting in persistent deactivation even at elevated temperature. Phosphate-induced inhibition of Fe redox sites is discussed by Park (2024).

For NaSHT, N_2O conversion remained negligible until approximately 380 °C and reached only ~19% at 500 °C. The delayed light-off and low plateau demonstrate severe inhibition of N–O bond activation. This confirms that sodium poisoning strongly deactivates redox-accessible iron sites and suppresses oxygen mobility required for N_2O decomposition. Alkali-induced suppression of Fe redox functionality has been reported previously (Liu et al. 2020).

For the HT catalyst, N_2O conversion initiated near 330–340 °C and reached approximately 70–75% at 500 °C. Hydrothermal ageing modifies Fe speciation and

reduces acidity, but redox-active iron centres capable of N–O bond activation remain present after steaming (Buttignol et al. 2022; Park 2024). The retained N_2O activity observed here is therefore consistent with partial structural ageing rather than complete redox deactivation.

5.2 DRIFTS

Diffuse Reflectance Infrared Fourier Transform Spectroscopy (DRIFTS) was used to examine surface species present on sulphur-aged and poisoned Fe–SCR catalysts. The measurements were performed in ambient air and temperature conditions without reaction mixtures. Consequently, the obtained spectra describe the surface state of the catalysts after ageing and poisoning treatments rather than reaction intermediates formed under operando SCR conditions. The DRIFTS spectra of all samples are presented in Figure 7.

In NH_3–SCR literature, DRIFTS measurements conducted under reaction or adsorption feeds commonly report coordinated NH_3 species on Lewis acid sites (1600–1500 cm^{-1}), NH_4^+ species bound to Brønsted acid sites (~1450 cm^{-1}), and nitrate or nitrite intermediates in the 1600–1500 cm^{-1} region formed during NO oxidation and SCR pathways (Busca et al. 1998; Yang et al. 2015; Qiu et al. 2020). These assignments provide a reference framework for interpreting catalyst surface functionalities; however, in the present study such bands are interpreted only as indicators of adsorption-capable surface environments, not as evidence of ongoing SCR reactions.

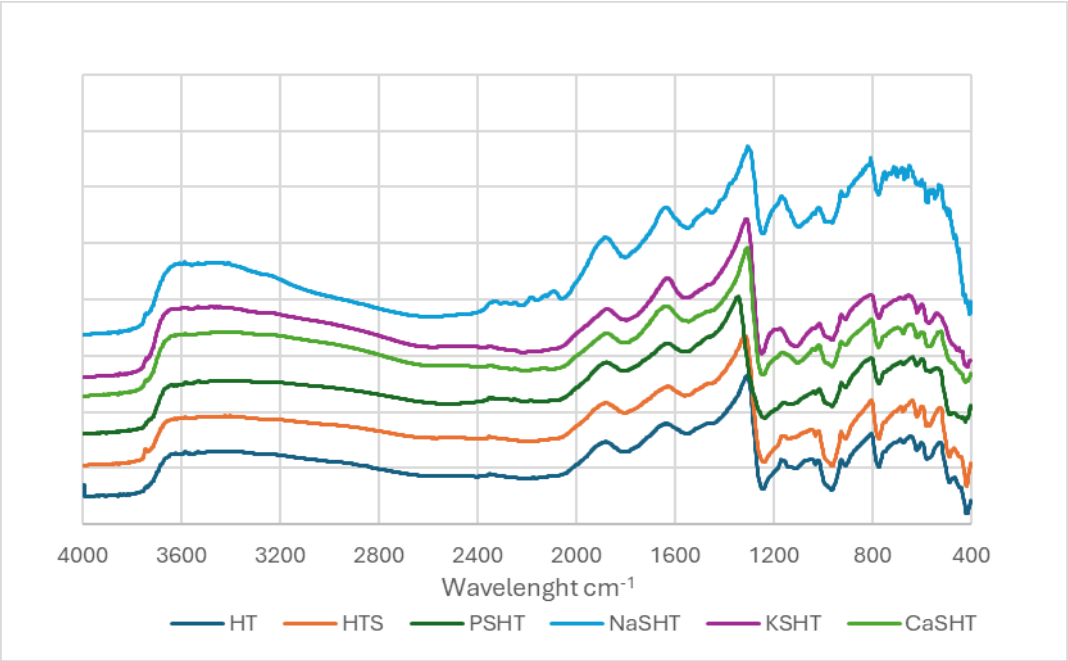

Figure 7. DRIFTS results for different samples.

All samples exhibit broad absorption bands in the 3700–3000 cm^{-1} region, corresponding to O–H stretching vibrations of surface hydroxyl groups and hydrogen-bonded water. The intensity of this region reflects surface hydroxylation and water retention, which influence ammonia adsorption by modifying Brønsted acidity and hydrogen-bonding interactions during SCR (Yang et al. 2015; Wang et al. 2019).

A band near 3640 cm^{-1} can be assigned to terminal hydroxyl groups associated with framework or extra-framework iron species. Variations in its intensity indicate changes in surface hydroxyl density after ageing or poisoning treatments (Yang et al. 2015). Increased intensity in alkali-treated samples is consistent with neutralization of acid sites and enhanced hydroxyl stabilization.

The broad band in 3600–3200 cm^{-1} corresponds to hydrogen-bonded molecular water adsorbed on the catalyst surface. Enhanced water-related absorption after alkali treatment suggests increased water retention due to reduced NH_3 adsorption capacity and decreased surface acidity (Wang et al. 2019).

In the 1700–1200 cm^{-1} region, several adsorption-related bands are observed that are commonly discussed in NH_3–SCR literature. A band near 1620 cm^{-1} is attributed to vibrations associated with coordinatively unsaturated Fe^{3+} centres interacting with adsorbed surface species and reflects the presence of acidic iron sites (Busca et al. 1998;

Yang et al. 2015). Suppression of this feature after alkali or phosphorus treatment indicates partial blockage or loss of accessible iron sites and reduced acidity.

The feature observed around 1450 cm^{-1} corresponds to vibrations typically assigned to acid sites (Busca et al. 1998; Miao et al. 2020). Variations in this band can be interpreted as changes in acidic environments resulting from poisoning and ageing treatments. The weakening of this feature after sodium treatment suggests neutralization of acid sites and diminished adsorption functionality.

A band or shoulder near 1550 cm^{-1} is commonly associated with nitrate-type surface species formed via NO oxidation on Fe-based SCR catalysts (Qiu et al. 2020). The reduced intensity observed after sulphur ageing suggests inhibition of oxidizable surface sites due to sulphate coverage. Nitrate species detected on surface are most likely originated from treatment solutions used.

Below 1200 cm^{-1}, the spectra are dominated by zeolite framework vibrations together with contributions originating from deposited poisoning species. After sulphur ageing, additional bands appear in the 1200–1000 cm^{-1} region, which are consistent with asymmetric S–O stretching vibrations of surface sulphate species (Yu et al. 2019; Qiu et al. 2020). Persistence of these bands confirms sulphate accumulation on the catalyst surface and associated blocking of catalytically relevant sites. Phosphorus-poisoned samples exhibit intense absorptions in the 1100–900 cm^{-1} region attributed to phosphate species and formation of iron phosphate structures known to block active Fe centres and induce largely irreversible catalyst deactivation (Yang et al. 2015; Miao et al. 2020).

Alkali-treated catalysts display pronounced spectral perturbations below 1000 cm^{-1}, indicating modification of the Fe–O lattice and disturbance of the zeolite framework environment. Alkali poisoning is widely reported to suppress acidity and adsorption capacity of Fe-based SCR catalysts (Yang et al. 2015).

Among the investigated samples, the hydrothermally aged (HT) catalyst retains relatively clear adsorption-related features in the 1600–1300 cm^{-1} region together with limited low-frequency perturbation, indicating preservation of accessible surface sites. In contrast, sulphur-aged samples exhibit strong sulphate-related bands accompanied by attenuation of adsorption-related features, consistent with partial surface site blocking. Potassium-

and calcium-modified samples retain detectable adsorption-related bands, suggesting partial preservation of adsorption functionality despite sulphate formation.

5.3 XRD

XRD analysis with coated catalyst samples demonstrated that the cordierite substrate remained the dominant crystalline phase in all investigated samples after hydrothermal sulphur ageing, regardless of the presence of additional elements (Na, P, Ca or K). The characteristic reflections at approximately $2\theta \approx 12°$ were consistently observed across all samples, together with multiple lower-intensity reflections in the 20–40° region. The persistence of these peaks indicates that the bulk crystallographic structure of cordierite was preserved under the applied hydrothermal sulphur ageing conditions. This confirms that the structural changes observed are attributable to the formation of secondary crystalline phases rather than degradation of the monolithic substrate.

In the sulphur-only aged sample (SHT), cordierite remained the clearly dominant phase, like in all the samples, and only minor additional crystalline phases were detected. The absence of intense sulphate or sulphide reflections suggests that sulphur was either present in highly dispersed form, amorphous deposits, or surface-bound species below the XRD detection limit. In Fe-based SCR catalysts, sulphur can form surface iron sulphates or, in low temperatures, ammonium sulphates that may remain poorly crystalline depending on ageing conditions (Ma et al. 2012; Zhang et al. 2019). The limited formation of bulk crystalline sulphur phases in SHT therefore suggests relatively weak sulphur-driven crystallization in the absence of alkali or alkaline earth metals.

In contrast, the sodium-containing sample (NaSHT) exhibited several intense reflections corresponding to sodium sulphate, indicating significant crystallization of Na_2SO_4. The strong peak intensities observed between approximately 22° and 36° suggest that sodium sulphate was present in relatively high abundance compared to secondary phases in SHT. In addition, β-Na_2S_5 reflections were identified for example in 21°, 23°, 26° and 34°, demonstrating the formation of sodium polysulfide species under hydrothermal sulphur ageing conditions. Sodium cobalt sulphate hydrate was also detected, indicating interaction between sodium, sulphur and transition metal species. The pronounced formation of sodium sulphates is consistent with the strong thermodynamic stability of

alkali metal sulphates and their well-documented role in SCR catalyst deactivation, where alkali metals neutralize Brønsted acid sites and promote sulphate accumulation (Putluru et al. 2011; Peng et al. 2015). The high relative peak intensities in NaSHT compared to SHT therefore indicate that sodium strongly enhances bulk sulphate crystallization.

The phosphorus-containing sample (PSHT) exhibited the most complex phase composition. In addition to cordierite, strong reflections corresponding to diadochite were observed across a wide angular range, suggesting substantial formation of mixed iron phosphate–sulphate phases. The broad distribution and multiplicity of reflections indicate that these phases were present in significant quantity. Furthermore, α-P_4S_3 for example in 20° and phosphorus oxide sulphide for example in 16° were detected, confirming the formation of mixed phosphorus–sulphur compounds. Ardealite was also identified through its characteristic reflection. The interaction of phosphorus species with active catalytic sites in selective catalytic reduction (SCR) materials often leads to the formation of phosphate compounds on the catalyst surface, which can block or alter active sites and thereby affect catalytic activity and deactivation behaviour. Phosphorus poisoning mechanisms in SCR catalysts have been linked to chemisorption and phosphate deposition that modify catalyst surfaces and active species, hindering reactant adsorption and redox processes critical for NH_3-SCR performance (Zhang 2024; Miao et al. 2020). The relative intensity and diversity of reflections in PSHT suggest that phosphorus significantly modifies sulphur chemistry, leading to the stabilization of multi-component crystalline compounds rather than simple alkali sulphates.

In the calcium-containing sample (CaSHT), calcium sulphide (most clearly in 36° and 52°) and anhydrite ($CaSO_4$) (most clearly in 29° and also in 36° and 45°) were clearly identified. The strong reflection of $CaSO_4$ indicates the formation of stable crystalline calcium sulphate, while additional reflections corresponding to CaS demonstrate partial sulphide formation. The simultaneous presence of CaS and $CaSO_4$ suggests parallel sulphide and sulphate formation pathways during hydrothermal ageing. Calcium sulphate is thermodynamically stable and can act as a sulphur trap; however, the formation of bulk $CaSO_4$ deposits may also contribute to pore blocking and surface coverage in SCR systems (Liu et al. 2010). Compared to NaSHT and PSHT, the phase diversity in CaSHT was lower, but the relative intensity of $CaSO_4$ reflections indicates significant sulphur immobilization in crystalline form.

The potassium-containing sample (KSHT) displayed multiple potassium-bearing phases, including potassium magnesium aluminium silicate (for example in 5°, 25°, 30° and 33°), potassium ammonium hydrogen sulphate (between 25°–40°), and potassium iron phosphate (in 37° an 34°). The strong reflection of potassium ammonium hydrogen sulphate suggests substantial crystallization of potassium sulphate species. Like sodium, potassium is known to neutralize acid sites and promote sulphate formation in Fe-based SCR catalysts, resulting in decreased NO_X conversion efficiency (Putluru et al. 2011; Peng et al. 2015). The detection of potassium iron phosphate further indicates interaction between potassium, phosphorus (if present in trace amounts), and iron species, potentially altering the active Fe environment.

A comparison of all samples reveals clear additive-dependent trends. Sulphur-only ageing resulted in minimal bulk crystalline sulphate formation, whereas alkali metals (Na and K) strongly promoted the crystallization of sulphates and sulphides, as evidenced by the higher number and intensity of corresponding reflections. Phosphorus led to the formation of complex iron phosphate–sulphate phases, indicating strong chemical interaction with Fe species. Calcium promoted the formation of stable $CaSO_4$ and CaS phases, suggesting effective sulphur trapping but with potential implications for pore blockage. Overall, the qualitative peak intensity trends suggest that the extent of crystalline phase formation follows approximately the order PSHT > NaSHT ≈ KSHT > CaSHT > SHT, indicating that phosphorus and alkali metals most strongly influence sulphur-related phase evolution in Fe-based SCR systems.

5.4 Specific surface area (BET)

Textural properties and specific surface area (S_{BET}) of the Fe-SCR catalysts were evaluated by N_2 physisorption (-196 °C) to assess the impact of hydrothermal aging and chemical poisoning on the zeolite support structure. Samples included Fe-zeolite together with cordierite substrate ($S_{BET} < 1$ m^2/g), which decreased the detected values. The fresh, coated Fe-SCR catalyst exhibited a BET surface area of 104 m^2/g and a micropore area of 79 m^2/g, indicating a well-preserved zeolitic pore network with high accessible internal surface area.

After hydrothermal aging, the BET surface area decreased to 67 m^2/g and the micropore area to 49 m^2/g, reflecting partial dealumination and collapse of the zeolite framework under high-temperature steam exposure. Interestingly, the hydrothermally aged sample subsequently exposed to sulphur retained a higher BET surface area of 84 m^2/g and micropore area of 63 m^2/g compared to hydrothermal aging alone, suggesting that sulphate species partially inhibit further structural degradation of the zeolite pores.

Phosphorus and sulphur co-poisoning caused the most severe loss of porosity, yielding a BET surface area of 58 m^2/g and micropore area of 43 m^2/g, consistent with pore blocking by phosphate and sulphate deposits within the zeolite channels. Alkali and alkaline earth metal poisoning showed intermediate effects: the KSHT-treated sample retained 80 m^2/g BET surface area, while CaSHT resulted in 69 m^2/g, indicating partial neutralization of Brønsted acid sites and moderate pore obstruction.

Textural properties of the Na- and S-poisoned Fe-SCR catalyst were also evaluated. The NaSHT sample exhibited a BET surface area of 49 m^2/g and a micropore area of 36 m^2/g, with an external surface area of 13 m^2/g and micropore volume of 0.019 cm^2/g. These values represent a substantial decrease compared to the fresh catalyst and indicate severe damage to the zeolite framework and extensive pore blocking caused by sodium and sulphur species. Alkali metals neutralize acid sites and promote framework dealumination, while sulphur compounds form sulphate deposits that further obstruct pore channels. The combined presence of Na and S therefore leads to accelerated collapse of the internal pore network.

Compared to other poisoned samples, the NaSHT-treated catalyst displays the most severe reduction in both BET surface area and micropore area. Whereas KSHT- and CaSHT-poisoned samples retained BET surface areas of approximately 80 m^2/g and 69 m^2/g, respectively, the NaSHT sample retains only about half of the surface area of the fresh catalyst, indicating that sodium is a particularly aggressive poison when combined with sulphur.

Overall, the reduction in micropore area across all poisoned samples confirms that deactivation of Fe-SCR catalysts is strongly associated with loss of accessible zeolite internal surface area, which directly limits the number of available isolated Fe active sites for NH_3-SCR reactions. In Table 7 BET surface areas, micropore areas, total pore volumes

and average pore widths of different samples are summed. Figure 8 illustrates BET surface areas of different samples.

Table 7. BET surface area, micropore area, total pore volume and average pore width for different samples including catalyst and cordierite substrate.

Sample	BET surface area (m^2/g)	Micropore area (m^2/g)	Total pore volume (cm^3/g)	Average pore width (nm)
Fresh	104	79	0.096	3.7
HT	67	49	0.07	4.2
HTS	84	63	0.091	4.3
PSHT	59	43	0.062	4.2
KSHT	80	58	0.085	4.3
CaSHT	69	51	0.065	3.8
NaSHT	49	36	0.053	4.3

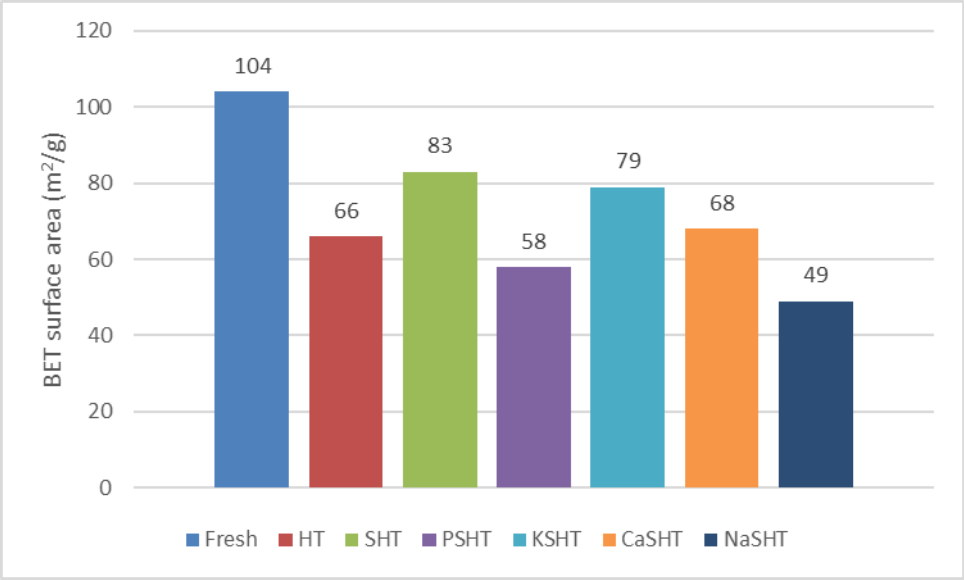

Figure 8. Effect of hydrothermal aging and chemical poisoning on BET surface area of Fe-SCR catalysts.

5.5 SEM

The surface chemical evolution of Fe-based selective catalytic reduction (Fe–SCR) catalysts subjected to hydrothermal ageing and subsequent exposure to sulphur and common biofuel-derived poisons (Ca, Na, K and P) was investigated using scanning

electron microscopy coupled with energy-dispersive X-ray spectroscopy (SEM–EDS). Localised elemental analyses reveal systematic sulphur accumulation, deposition of alkali and alkaline earth elements, and heterogeneous redistribution of Fe species. The aluminosilicate matrix remains dominant in all samples, while clear compositional modifications are observed following sulphur and poison exposure.

General matrix composition

All samples exhibit a dominant aluminosilicate composition characterised by high oxygen, silicon and aluminium contents. Oxygen concentrations range approximately between 40–47 wt%, silicon between 35–45 wt%, and aluminium between 8–20 wt%. This composition is consistent with an aluminosilicate washcoat typical of Fe–SCR catalysts (Busca 2007; Iwamoto and Hamada 1991). Iron is detected in all samples, typically between 0.5–4.5 wt%, with clear variation between analysed spots. This indicates heterogeneous distribution of Fe species within the washcoat layer, which is consistent with the known dispersion behaviour of exchanged and extra-framework iron in aluminosilicate catalysts (Brandenberger et al. 2008). In some measurement points, magnesium concentrations of approximately 8–9 wt% are observed, suggesting local exposure of the cordierite-type substrate beneath the washcoat layer.

Hydrothermally aged sample (HT)

The hydrothermally aged reference sample shows a stable aluminosilicate matrix without significant sulphur or alkali contamination. Iron is present at relatively low concentrations in several spectra, indicating possible redistribution following ageing. Localised reductions in aluminium content suggest limited dealumination of the framework. Hydrothermal ageing of aluminosilicate catalysts is known to induce framework dealumination and migration of metal species, particularly under high-temperature steam conditions (Moulijn et al. 2013; Brandenberger et al. 2008).

Hydrothermally aged with sulphur (SHT)

Sulphur exposure results in measurable sulphur concentrations, typically up to approximately 1–2 wt% in localised regions. The sulphur distribution is heterogeneous, indicating non-uniform surface deposition. In several spectra, sulphur enrichment

coincides with increased iron content. The formation of iron sulphate species or sulphate deposition near iron-rich domains is therefore plausible. Sulphation of transition metal sites under SCR conditions has been widely reported, and sulphate formation is known to modify surface acidity and redox properties (Busca 2007; Nova and Tronconi 2014). The data indicates that sulphur contributes to surface modification and potential partial blocking of active sites. Elemental mapping of sulphur in hydrothermally aged and sulphur poisoned sample is show on the Figure 9.

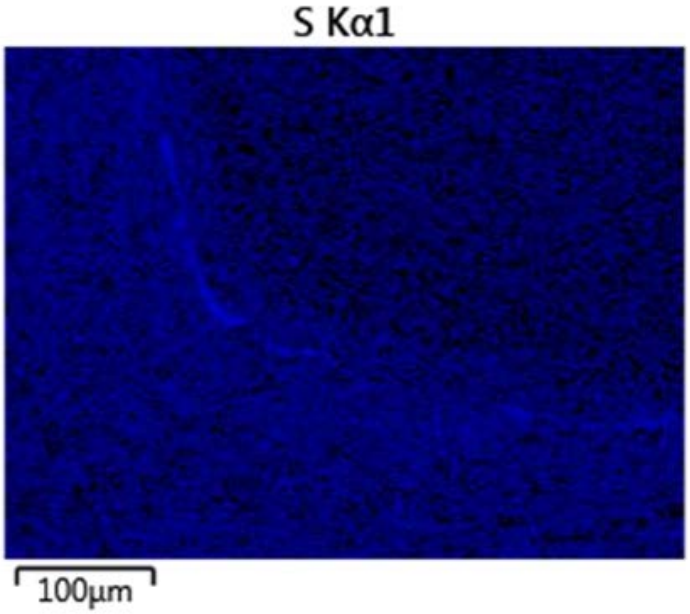

Figure 9. SEM–EDS elemental mapping of sulphur in HTS catalyst sample.

Hydrothermally aged with sulphur and calcium (CaSHT)

The calcium-containing sample exhibits calcium concentrations up to approximately 2–3 wt% in analysed regions. Sulphur remains present at comparable levels. The frequent co-occurrence of Ca and S strongly suggests formation of calcium sulphate-type deposits. Calcium is known to react readily with sulphur species under exhaust conditions, forming thermally stable $CaSO_4$ phases (Forzatti and Lietti 1999; Nova and Tronconi 2014). The Ca–S-rich regions observed here are therefore consistent with sulphate deposition. Such deposits can block pore entrances and reduce accessibility to active sites. In addition, alkaline earth metals are known to neutralise acidic sites in aluminosilicate catalysts, thereby suppressing SCR activity (Busca 2007; Moulijn et al. 2013). In Figure 10 elemental mapping of Ca is shown for the CaSHT sample.

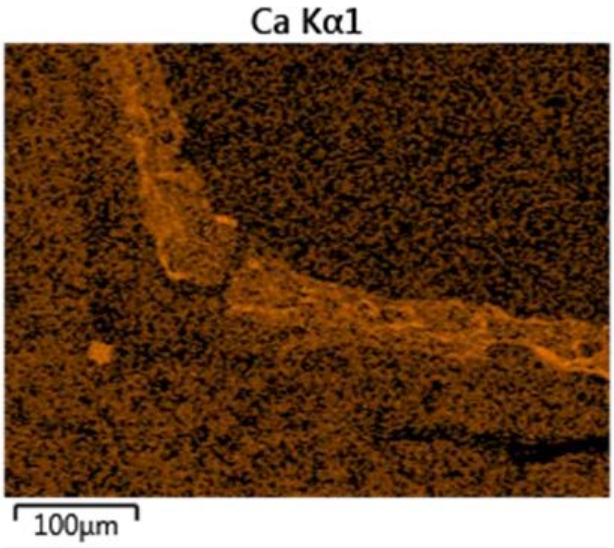

Figure 10. SEM–EDS elemental mapping of calcium in CaSHT catalyst sample.

Hydrothermally aged with sulphur and sodium (NaSHT)

In the sodium-containing catalyst, sodium concentrations reach up to approximately 2–3 wt% in certain spectra. Sulphur remains detectable at moderate levels. Sodium distribution is heterogeneous, indicating localised surface enrichment. Sodium is well known to exchange with surface acid sites in aluminosilicate materials, leading to neutralisation of acidity (Iwamoto and Hamada 1991; Busca 2007). The observed Na enrichment is therefore consistent with ion-exchange processes. The coexistence of sodium and sulphur suggests possible formation of Na_2SO_4 species under sulphur-rich conditions (Forzatti and Lietti 1999). Alkali metals are particularly detrimental to SCR catalysts due to their strong basic character and their ability to suppress ammonia adsorption and activation (Nova and Tronconi 2014). Figure 11 shows the Na elemental mapping for the NaSHT sample.

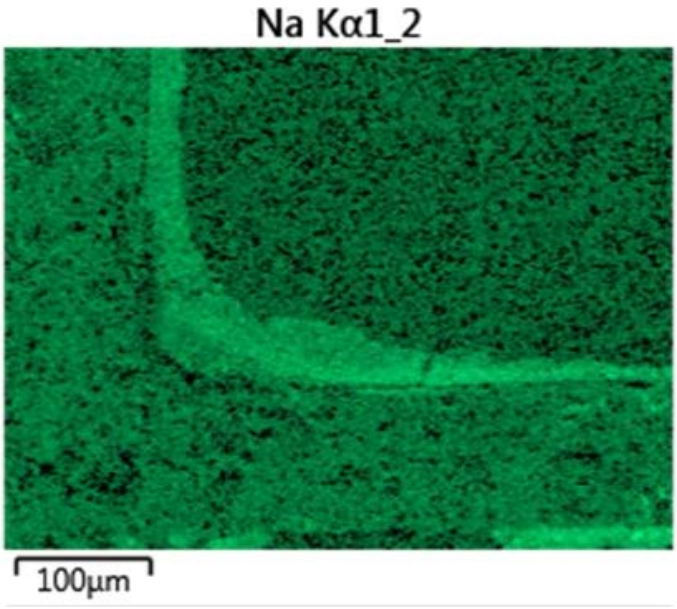

Figure 11. SEM–EDS elemental mapping of sodium in NaSHT catalyst sample.

Hydrothermally aged with sulphur and potassium (KSHT)

The potassium-exposed sample shows potassium concentrations up to approximately 1–2 wt% in selected regions. Sulphur remains present, and iron concentrations vary locally between approximately 1–4 wt%. Potassium behaves similarly to sodium in aluminosilicate systems, undergoing ion exchange with acidic sites and forming sulphate species under sulphur exposure (Busca 2007; Forzatti and Lietti 1999). The heterogeneous distribution observed here indicates localised poisoning rather than uniform surface coverage. Due to its larger ionic radius and strong basicity, potassium is often reported to induce severe deactivation of SCR catalysts through acid site neutralisation (Nova and Tronconi 2014). The elemental distribution of K in the KSHT sample is shown in Figure 12.

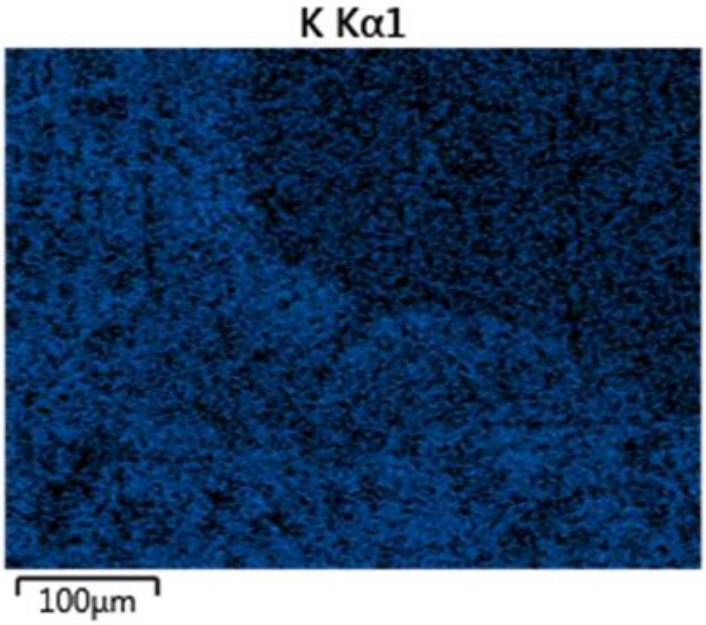

Figure 12. SEM–EDS elemental mapping of potassium in KSHT catalyst sample.

Hydrothermally aged with sulphur and phosphorus (PSHT)

Phosphorus is detected at relatively low concentrations in the analysed spectra. However, localised enrichment is observed in certain regions. Phosphorus was found mainly on the top layer of the catalyst. Phosphorus is known to interact strongly with aluminosilicate frameworks, forming aluminium phosphate species and modifying the coordination environment of framework aluminium (Blasco et al. 2006; Moulijn et al. 2013). Unlike alkali metals, phosphorus does not primarily act through simple ion exchange but rather through chemical modification of the framework structure. Even relatively low phosphorus concentrations can therefore induce irreversible changes in acidity and structural integrity (Blasco et al. 2006). Sulphur is present at moderate levels but does not show strong co-localisation with phosphorus, suggesting that phosphorus predominantly interacts with the framework rather than forming simple sulphate phases. Figure 12 presents the elemental mapping of P for the PSHT sample.

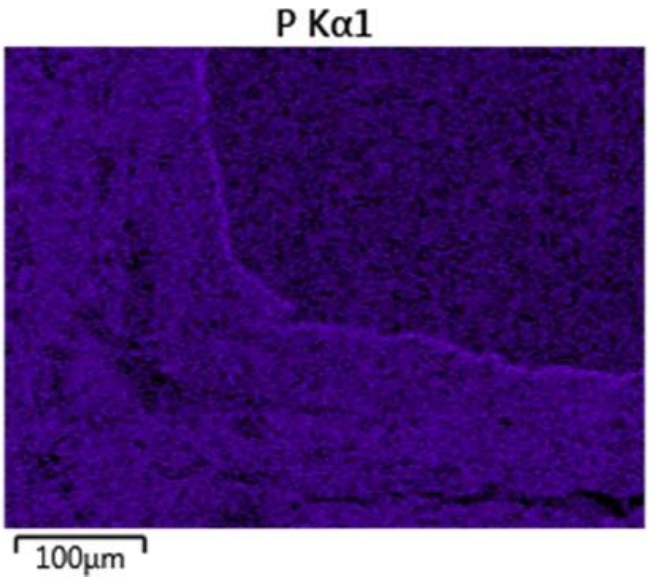

Figure 13. SEM–EDS elemental mapping of phosphorus in PSHT catalyst sample.

5.5.1 Inlet-Outlet surface composition in double-poisoned catalysts

SEM–EDS analysis was performed on both inlet and outlet ends of the double-poisoned catalysts (CaSHT, NaSHT, KSHT, PSHT) to evaluate axial distribution of deposited species. The aluminosilicate matrix remains dominant in both inlet and outlet ends. However, compositional gradients are observed for sulphur and poisoning elements. Measured element concentrations are presented in Table 8.

In the CaSHT sample, higher Ca and S concentrations are generally observed at the inlet, and Ca–S co-localisation is more pronounced in this end. This suggests preferential sulphate formation near the gas-entry zone, which is consistent with diffusion-limited deposition phenomena commonly observed in monolithic catalysts (Moulijn et al. 2013).

In the NaSHT and KSHT samples, Na and K are detected in both inlet and outlet regions. Although inlet concentrations are often slightly higher, alkali elements appear more broadly distributed than calcium. This behaviour is consistent with the higher mobility of alkali cations and their ability to penetrate deeper into porous aluminosilicate structures through ion-exchange processes (Busca 2007).

In the PSHT sample, phosphorus enrichment is localised and does not exhibit strong sulphur co-localisation. The axial distribution suggests non-uniform deposition and potential preferential fixation near the gas-entry region.

Overall, the inlet–outlet comparison indicates spatially non-uniform poisoning, with inlet regions generally exhibiting more pronounced contamination. Such axial gradients are typical in monolithic catalytic systems exposed to contaminant-containing gas streams (Moulijn et al. 2013).

Table 8. Measured concentrations (inlet-outlet) of the aged samples.

Summary (wt-%)	PSHT-IN			PSHT-OUT			CaSHT-IN			CaSHT-OUT		
Element	Whole	Bottom	Top	Whole	Bottom	Top	Whole	Bottom	Top	Whole	Bottom	Top
O	43.9	43.3	45.3	44.3	44.1	44.2	44.4	45.1	45.0	44.1	43.3	45.9
Na	0.1	0.2	0.1	0.1	0.1	0.1	0.1	0.1	0.2	0.1	0.1	0.1
P	1.7	1.6	7.4	0.2	0.2	1.7	0.0	0.0	0.0	0.0	0.0	0.0
S	0.6	0.5	0.1	0.3	0.3	0.2	8.1	9.5	6.8	1.6	3.1	2.2
K	0.1	0.1	0.0	0.0	0.0	0.1	0.0	0.1	0.1	0.1	0.0	0.0
Ca	0.0	0.0	0.0	0.0	0.0	0.0	7.7	9.6	6.8	1.6	3.2	2.4

Summary (wt-%)	KSHT-IN			KSHT-OUT			NaSHT-IN			NaSHT-OUT		
Element	Whole	Bottom	Top	Whole	Bottom	Top	Whole	Bottom	Top	Whole	Bottom	Top
O	46.7	47.5	43.3	44.8	43.8	43.4	43.0	42.0	48.2	45.1	42.6	46.7
Na	0.3	0.5	0.5	0.1	0.1	0.2	4.0	5.7	1.8	1.4	3.9	2.2
P	0.0	0.2	0.2	0.0	0.0	0.0	0.0	0.0	0.0	0.0	0.0	0.0
S	0.4	1.1	0.3	0.7	0.7	0.8	2.5	3.4	0.8	0.8	2.0	1.1
K	17.0	24.6	17.5	0.1	0.1	0.1	0.7	0.9	0.0	0.0	0.2	0.0
Ca	0.7	0.6	1.0	0.0	0.0	0.0	0.0	0.0	0.0	0.0	0.0	0.0

6 CONCLUSIONS

Comparison of the NO_X, NH_3, and N_2O conversion profiles reveals consistent trends across all poisoned catalysts, indicating that the poisons primarily affect drastically common surface functionalities governing both NH_3 adsorption and active sites. Potassium- and calcium-modified samples retain higher activity after sulphur ageing, whereas sodium and phosphorus cause severe deactivation beyond sulphur poisoning. The identical activity ranking across NO_X, NH_3, and N_2O conversions (KSHT > CaSHT > SHT > PSHT > NaSHT) highlights active catalyst surface and NH_3 adsorption as key controlling steps in SCR performance.

Potassium preserves NH_3 adsorption capacity and a significant fraction of active iron sites, leading to higher NH_3, NO_X and N_2O conversions in comparison to poison free Fe-SCR catalyst. Calcium provides moderate recovery of activity by mitigating sulphur-induced site blocking but does not fully restore redox cycling. In contrast, phosphorus poisoning causes persistent suppression of NH_3 oxidation and SCR functionality, while sodium produces the most severe deactivation by nearly eliminating NO_X conversion activity based on NH_3 adsorption and accessible iron centres.

DRIFTS measurements provide molecular-level evidence supporting these catalytic trends. Strong phosphate and sulphate bands correlate with site blocking and redox suppression, consistent with literature on SCR catalyst poisoning (Forzatti 2001; Yang et al. 2015).

The catalytic activity measurements correlate strongly with changes in textural properties of the zeolite support. N_2 physisorption results demonstrate that hydrothermal aging and chemical poisoning lead to progressive loss of BET surface area and microporosity, indicating structural degradation and pore blocking of the zeolite framework. The fresh Fe-SCR catalyst exhibits high BET surface area and micropore area, consistent with a well-preserved zeolitic pore network providing abundant accessible iron active sites. Among the poisoned samples, sodium and phosphorus cause the most severe losses of microporosity, while potassium and calcium show intermediate effects.

Alkali metals neutralize acid sites and promote dealumination, while sulphur and phosphorus form deposits that block channels and hinder diffusion to internal Fe sites.

Consequently, structural collapse and pore obstruction directly translate into reduced NH_3 uptake and limited availability of active iron sites.

The XRD results provide complementary structural evidence that directly supports the activity, DRIFTS and textural observations. In all samples, the cordierite reflections remained unchanged after hydrothermal sulphur ageing, confirming that the monolithic substrate preserved its crystallographic integrity. This agrees with the BET results showing that deactivation was caused by changes occurring within the zeolitic active phase and by deposition of secondary species. In the sulphur-only aged sample, sulphur was predominantly present as highly dispersed or amorphous surface species. This is consistent with the moderate decrease in adsorption bands observed by DRIFTS and the intermediate catalytic activity of the S-only sample.

In contrast, sodium- and phosphorus-modified samples exhibited the highest number and intensity of additional crystalline reflections, which directly correlates with their severe activity loss. The NaSHT catalyst showed intense sodium sulphate and polysulphide phases. Such bulk sulphate formation is consistent with the pronounced loss of surface acidity observed by DRIFTS and the severe decrease in microporous surface area measured by N_2 physisorption, indicating that sulphate-assisted pore blocking and acid site neutralization occur simultaneously. Similarly, the phosphorus-containing sample exhibited multiple iron phosphate–sulphate phases, supporting the observed suppression of SCR and NH_3 oxidation functionality. In comparison, potassium- and calcium-modified samples showed fewer and less intense secondary crystalline phases, which aligns with their better preservation of microporosity, and higher NO_X conversion. Thus, the XRD data provide structural confirmation that the severity of sulphate and phosphate formation parallels the observed catalytic deactivation trend (KSHT < CaSHT < SHT < PSHT < NaSHT), linking bulk phase evolution with chemical site poisoning and pore accessibility loss.

Comparison with literature reveals some differences in reported poisoning strength. Lisi and Cimino (2020) reported alkali poisoning severity in the order K > Na > Ca > Mg over various SCR catalysts, attributing deactivation primarily to acid site loss and decreased reducibility. In contrast, the present study identifies sodium as the most aggressive poison when combined with sulphur ageing. This discrepancy likely arises from differences in experimental conditions: Lisi and Cimino investigated fresh catalysts under single-metal

poisoning without prior hydrothermal ageing at 500 °C or sulphur exposure, whereas the present work combines hydrothermal ageing and sulphur treatment before alkali addition. Under these harsher conditions, sodium-induced dealumination and sulphate-assisted pore blocking synergistically accelerate zeolite framework collapse, explaining the stronger deactivation observed here.

SEM–EDS analysis provides direct microstructural confirmation of the deactivation mechanisms inferred from activity, DRIFTS, BET and XRD results. The dominant aluminosilicate matrix was preserved in all samples, confirming that bulk support collapse was not responsible for activity loss. However, a high surface enrichment of sulphur and poisoning elements was observed particularly in inlet zone, together with dropped access or number of iron sites. In the Ca- and K-containing samples, sulphur was frequently co-localised with the respective cations, indicating formation of metal sulphate-type surface species. In contrast, Na and P samples showed more extensive and heterogeneous accumulation of poisoning elements, particularly at inlet regions, supporting the presence of axial gradients and severe surface contamination. The pronounced Na enrichment and co-presence with sulphur are consistent with formation of alkali sulphates and strong acid site neutralisation, while localised phosphorus enrichment supports framework modification through phosphate formation (Blasco et al. 2006; Busca 2007). The SEM results therefore provide spatial evidence that the most severe catalytic deactivation correlates with the highest degree of surface contamination, sulphate/phosphate deposition and a loss of Fe active sites. The inlet–outlet gradients further demonstrate that poisoning is not uniform across the monolith, which is characteristic of diffusion-limited deposition phenomena in practical SCR systems (Moulijn et al. 2013). Together with spectroscopic and textural results, the SEM findings confirm that Fe-SCR durability under multi-poison ageing is governed by coupled chemical site blocking and progressive loss of accessible internal surface area.

Overall, the combined activity, DRIFTS, BET, XRD and SEM results demonstrate that Fe-SCR catalyst deactivation is governed by both chemical site poisoning and physical loss of accessible internal surface area. Preservation of zeolite microporosity is therefore a key factor controlling long-term Fe-SCR durability under realistic hydrothermal and multi-poison ageing conditions. In the future, it is useful to repeat the activity experiment up to 500 °C to see if deactivation is partly reversible.

7 SUMMARY

The increasing use of bio-based fuels introduces new impurity profiles into exhaust gas streams, including sulphur, alkali and earth-alkali metals, and phosphorus. These contaminants can significantly affect the durability and performance of selective catalytic reduction (SCR) catalysts used for NO_X abatement. Understanding the catalyst deactivation under such conditions is essential for ensuring long-term environmental compliance and cost-effective operation of emission control systems.

This Master's thesis investigates the deactivation behaviour of SCR catalysts based on the Fe-Beta zeolite. While the literature section reviews the fundamental principles of SCR catalysis and discusses both Fe- and V-based catalyst systems, the experimental work of this thesis focuses exclusively on Fe-SCR. The objective was to determine how impurities originating from bio-based fuels influence catalyst activity, surface chemistry, and structural stability, and to identify the dominant deactivation mechanisms.

Catalytic performance was evaluated using NO_X, NH_3, and N_2O conversion measurements. Surface interactions and adsorption properties were examined using Diffuse Reflectance Infrared Fourier Transform Spectroscopy (DRIFTS). Morphological changes were analysed using Brunauer–Emmett–Teller surface area (BET) measurements, structural modifications were investigated by X-ray diffraction (XRD), and elemental distributions were characterised using scanning electron microscopy coupled with energy-dispersive spectroscopy (SEM–EDS).

The results demonstrate that catalyst deactivation under multi-poison conditions is governed by two closely connected mechanisms: chemical site poisoning and physical loss of microporous surface area. Chemical poisoning suppresses acidity and reduces the availability of SCR active iron sites, while structural degradation and pore blocking decrease accessibility to internal active sites.

The activity in SCR and N_2O removal reactions followed the order: KSHT > CaSHT > SHT > PSHT > NaSHT. All these poisons caused a severe deactivation for SCR activity. Sodium and phosphorus caused the most severe deactivation. In these samples, DRIFTS analysis indicated loss of surface acidity. BET measurements revealed significant reduction in microporous surface area, confirming a loss of active catalyst surface in

zeolite framework. XRD analysis indicated the formation of secondary sulphate and phosphate phases, while SEM–EDS showed heterogeneous surface enrichment and axial gradients within the catalyst monolith.

In contrast, potassium- and calcium-modified samples retained higher catalytic activity after sulphur ageing. These catalysts preserved a larger fraction of accessible iron acid sites and exhibited a less severe loss of microporosity. The combined results indicate that maintenance of active sites and microporous accessibility is critical for sustaining Fe-SCR performance. The study confirmed that deactivation is not caused by collapse of the cordierite support structure. The observed inlet–outlet gradients indicate that poisoning is spatially non-uniform, which correlated to practical operating conditions with monolithic catalysts.

Overall, this study provides information into how impurities derived from bio-based fuels caused severe decrease of Fe-zeolite catalyst activity. The findings emphasise the importance of preserving surface acidity, accessible active sites and microporous structure under hydrothermal and multi-poison ageing conditions. These results contribute to the development of more robust SCR systems suitable for future renewable fuel applications.

REFERENCES

Abdul Nasir, J., Morgan, K., Jenkins, R., Golunski, S. and Hutchings, G.J. (2024) 'The role of iron in zeolite Beta for deNOx catalysis', Journal of Catalysis, 429, pp. 1–15. Available at: https://orca.cardiff.ac.uk/id/eprint/172205

Agote-Arán, M., Jacobsen, V.V., Elsener, M., Schütze, F.W., Schilling, C.M., Katsaounis, E., Kröcher, O. and Ferri, D. (2023) 'Thermal sintering and phosphorus poisoning of a layered diesel oxidation catalyst', Topics in Catalysis, 66, pp. 777–786. doi: 10.1007/s11244-022-01752-w.

Al-Zubaidi, I. and Yang, C. (2020) 'Waste management of spent petroleum refinery catalyst', European Journal of Engineering Research and Science, 5(8), pp. 1–8.

Anastas, P.T. and Warner, J.C. (1998) Green Chemistry: Theory and Practice. Oxford: Oxford University Press.

Anekwe, I.M.S. and Isa, Y.M. (2025) 'Unlocking catalytic longevity: A critical review of catalyst deactivation pathways including coking, poisoning, thermal degradation and mechanical damage', RSC Advances [online]. Available at: https://pubs.rsc.org/en/content/articlehtml/2025/ya/d5ya00015g (Accessed: 4 December 2025).

Argyle, M.D. and Bartholomew, C.H. (2015) 'Heterogeneous catalyst deactivation and regeneration: A review', Catalysts, 5(1), pp. 145–269.

Bartholomew, C.H. (2001) 'Mechanisms of catalyst deactivation', Applied Catalysis A: General, 212(1–2), pp. 17–60. doi: 10.1016/S0926-860X(00)00843-7.

Bian, X. (2024) 'TiO_2-supported catalysts in low-temperature selective catalytic reduction (NH3-SCR): performance and H2O/SO2 resistance', Catalysts, 14(9), p. 558.

Blasco, T., Corma, A., Martínez-Triguero, J. and Martínez, A. (2006) 'Phosphorus-modified zeolite catalysts', Journal of Catalysis, 237, pp. 267–277.

Bobba, S., Carrara, S., Huisman, J., Mathieux, F. and Pavel, C. (2020) Critical raw materials for strategic technologies and sectors in the EU. Luxembourg: European Commission, JRC Science for Policy Report.

Bulavchenko, O.A. and Vinokurov, Z.S. (2023) 'In situ X-ray diffraction as a basic tool to study oxide and metal oxide catalysts', Catalysts, 13(11), p. 1421. doi: 10.3390/catal13111421.

Brandenberger, S., Kröcher, O., Tissler, A. and Althoff, R. (2008) 'The state of the art in selective catalytic reduction of NOx by ammonia using metal-exchanged zeolite catalysts', Catalysis Reviews, 50(4), pp. 492–531. doi: 10.1080/01614940802480122.

Brandenberger, S., Kröcher, O., Casapu, M., Tissler, A. and Althoff, R. (2011) 'Hydrothermal deactivation of Fe-ZSM-5 catalysts for the selective catalytic reduction of NO with NH3', Applied Catalysis B: Environmental, 101(3), pp. 649–659.

Brundtland, G.H. (1987) Our Common Future: Report of the World Commission on Environment and Development. New York: United Nations.

Burch, R. (2010) 'Knowledge and know-how in emission control catalysis', Topics in Catalysis, 53, pp. 1021–1031. Available at: https://doi.org/10.1081/CR-200036718 (Accessed: 15 July 2025).

Busca, G., Lietti, L., Ramis, G. and Berti, F. (1998) 'Chemical and mechanistic aspects of the selective catalytic reduction of NOx by ammonia over oxide catalysts: A review', Applied Catalysis B: Environmental, 18(1–2), pp. 1–36.

Buttignol, F., Morra, E., Arosio, F., Groppi, G. and Tronconi, E. (2022) 'Aging of industrial Fe-zeolite based catalysts for nitrous oxide reduction: Structural and catalytic implications', Catalysis Science & Technology, 12(6), pp. 1629–1641. doi: 10.1039/D2CY01486F.

Cao, Y., Han, F., Wang, M., Han, L., Zhang, C., Wang, J., Bao, W. and Chang, L. (2019) 'Regeneration of the waste selective catalytic reduction denitrification catalyst by nitric

acid washing', ACS Omega, 4(15), pp. 16629–16637. Available at: https://pubs.acs.org/doi/10.1021/acsomega.9b02288.

Cavelius, P., Vogel, M., Treu, L. and Angelidaki, I. (2023) 'The potential of biofuels from first to fourth generation', Frontiers in Energy Research, 11 [online]. Available at: https://www.ncbi.nlm.nih.gov/pmc/articles/PMC10063169/ (Accessed: 4 July 2025).

Chee, S.W. et al. (2023) 'Operando electron microscopy of catalysts: the missing cornerstone in heterogeneous catalysis research', Chemical Reviews.

Chen, L., Li, J. and Ge, M. (2017) 'The poisoning effect of phosphorus on Fe-based SCR catalysts and its influence on surface acidity', Applied Catalysis B: Environmental, 206, pp. 240–249. doi: 10.1016/j.apcatb.2017.01.040.

Chen, J., Liu, Z., Li, J. and Wang, Y. (2022) 'A review on the characterization of metal active sites over Cu-based and Fe-based zeolites for NH_3-SCR', RSC Advances, 12, pp. 27746–27765. doi: 10.1039/D2RA05107A.

Chen, Z. et al. (2024) 'Recent advances in SCR systems of heavy-duty diesel vehicles—low-temperature NOx reduction technology and combination of SCR with remote OBD', Atmosphere, 15(8), p. 997. Available at: https://www.mdpi.com/2073-4433/15/8/997 (Accessed: 10 February 2026).

Cheng, Y., Lambert, C., Kim, D.H., Kwak, J.H., Cho, S.J. and Peden, C.H.F. (2010) 'The different impacts of SO_2 and SO_3 on Cu/zeolite SCR catalysts', Catalysis Today, 151(3–4), pp. 266–270. doi: 10.1016/j.cattod.2010.01.013.

Cornejo, I., Nikrityuk, P. and Hayes, R.E. (2020) 'Heat and mass transfer inside of a monolith honeycomb', Catalysis Today, 383, pp. 193–206.

Cornejo, I., Nikrityuk, P. and Hayes, R.E. (2021) 'A review of the critical aspects in the multi-scale modelling of catalytic monolith reactors', Catalysts, 11(1), p. 89.

Colombo, M., Nova, I. and Tronconi, E. (2010) 'A comparative study of the NH_3-SCR reactions over a Cu-zeolite and a Fe-zeolite catalyst', Catalysis Today, 151(3–4), pp. 223–230.

Cullity, B.D. and Stock, S.R. (2014) Elements of X-ray Diffraction. 3rd edn. Harlow: Pearson.

Directive (EU) 2023/2413 of the European Parliament and of the Council of 18 October 2023 amending Directive (EU) 2018/2001, Regulation (EU) 2018/1999 and Directive 98/70/EC as regards the promotion of energy from renewable sources, and repealing Council Directive (EU) 2015/652 (2023) Official Journal of the European Union, 31 October, pp. 1–115.

European Commission (2020) The European Green Deal. Brussels: European Commission. Available at: https://commission.europa.eu/strategy-and-policy/priorities-2019-2024/european-green-deal_en (Accessed: 2 July 2025).

European Commission (2021) Euro 6/7 emission standards. Brussels: European Commission. Available at: https://ec.europa.eu/environment/air/transport/road.htm (Accessed: 15 July 2025).

European Commission (no date) Renewable Energy Directive – Targets and rules. Available at: https://energy.ec.europa.eu/topics/renewable-energy/renewable-energy-directive-targets-and-rules/renewable-energy-directive_en (Accessed: 4 December 2025).

European Parliament and Council (2023) Directive (EU) 2023/2413 of the European Parliament and of the Council of 18 October 2023 on the promotion of the use of energy from renewable sources. Official Journal of the European Union. Available at: https://eur-lex.europa.eu/eli/dir/2023/2413/oj (Accessed: 4 December 2025).

EPA (2014) EPA regulations for emissions durability of light-duty vehicles. United States Environmental Protection Agency. Available at: https://www.ecfr.gov/current/title-40/chapter-I/subchapter-C/part-86 (Accessed: 15 July 2025).

EPA (2023) Tier 3 Motor Vehicle Emission and Fuel Standards. United States Environmental Protection Agency.

European Environment Agency (EEA) (2021) Air Quality in Europe – 2021 Report. Luxembourg: Publications Office of the European Union. Available at: https://www.eea.europa.eu/publications/air-quality-in-europe-2021 (Accessed: 9 July 2025).

EVS (2023) EVS-EN 15940:2023 – Automotive fuels – Paraffinic diesel fuel from synthesis or hydrotreatment – Requirements and test methods. Estonian Centre for Standardisation. Available at: https://www.evs.ee/en/evs-en-15940-2023 (Accessed: 4 December 2025).

Farrauto, R.J. and Bartholomew, C.H. (2006) Fundamentals of Industrial Catalytic Processes. 2nd edn. Hoboken: Wiley.

Forzatti, P. and Lietti, L. (1999) 'Catalyst deactivation', Catalysis Today, 52(2–3), pp. 165–181. doi: 10.1016/S0920-5861(99)00074-7.

Forzatti, P. (2001) 'Present status and perspectives in de-NOx SCR catalysis', Applied Catalysis A: General, 222(1–2), pp. 221–236.

Gao, F., Kwak, J.H., Szanyi, J. and Peden, C.H.F. (2013) 'Current understanding of Cu- and Fe-exchanged chabazite molecular sieves for use as commercial diesel engine deNOx catalysts', Topics in Catalysis, 56, pp. 1441–1459.

Gao, F., Walter, E.D., Kollar, M., Wang, Y., Szanyi, J. and Peden, C.H.F. (2013a) 'Understanding the activity and deactivation of Cu/SSZ-13 for the selective catalytic reduction of NO with NH_3', Applied Catalysis B: Environmental, 136–137, pp. 338–346. doi: 10.1016/j.apcatb.2013.01.048.

Gao, F., Kwak, J.H., Szanyi, J. and Peden, C.H.F. (2013b) 'Current understanding of Cu-exchanged chabazite molecular sieves for use as commercial diesel engine deNOx catalysts', Topics in Catalysis, 56, pp. 1441–1459. doi: 10.1007/s11244-013-0108-8.

Gao, F., Zheng, Y., Kukkadapu, R.K., Wang, Y., Walter, E.D., Schwenzer, B., Szanyi, J. and Peden, C.H.F. (2016a) 'Iron loading effects in Fe/SSZ-13 NH_3-SCR catalysts: nature

of the Fe ions and structure–function relationships', ACS Catalysis, 6(5), pp. 2939–2954. doi: 10.1021/acscatal.6b00647.

Gao, F., Szanyi, J., Wang, Y., Schwenzer, B., Kollár, M. and Peden, C.H.F. (2016b) 'Hydrothermal aging effects on Fe/SSZ-13 and Fe/Beta NH_3–SCR catalysts', Topics in Catalysis, 59, pp. 882–886. doi: 10.1007/s11244-016-0563-5.

Gao, F., Kwak, J.H., Szanyi, J. and Peden, C.H.F. (2018) 'Current understanding of Fe-based catalysts for selective catalytic reduction of NOx with NH3', Catalysis Today, 320, pp. 55–68. doi: 10.1016/j.cattod.2018.03.048.

Gao, F. (2020) 'Fe-exchanged small-pore zeolites as ammonia selective catalytic reduction (NH_3-SCR) catalysts', Catalysts, 10(11), p. 1324. doi: 10.3390/catal10111324.

Geissdoerfer, M., Savaget, P., Bocken, N. and Hultink, E. (2017) 'The circular economy – A new sustainability paradigm?', Journal of Cleaner Production, 143, pp. 757–768.

Gelmini, S., Hoffman, M.A. and Onori, S. (2021) 'Design and experimental validation of three-way catalyst age estimator and oxygen storage capacity dynamics', SAE Technical Paper, 2021-24-0083.

Gong, J., Wang, D., Li, J., Kamasamudram, K., Currier, N. and Yezerets, A. (2019) 'An experimental and kinetic modeling study of aging impact on surface and subsurface oxygen storage in three-way catalysts', Catalysis Today, 320, pp. 83–92.

Govender, S. and Friedrich, H.B. (2017) 'Monoliths: A review of the basics, preparation methods and their applications to wastewater treatment', Catalysts, 7(2), p. 62. doi: 10.3390/catal7020062.

Goldstein, J.I., Newbury, D.E., Michael, J.R., Ritchie, N.W.M., Scott, J.H.J. and Joy, D.C. (2018) Scanning Electron Microscopy and X-ray Microanalysis. 4th edn. Cham: Springer.

Gregg, S.J. and Sing, K.S.W. (1982) Adsorption, Surface Area and Porosity. 2nd edn. London: Academic Press.

Guillén Hurtado, N., Rico-Pérez, V., García-García, A., Lozano-Castelló, D. and Bueno-López, A. (2012) 'Three-way catalysts: past, present and future', Dyna, Special Issue, pp. 115–128.

Guo, K., Ji, J. and Song, W. (2021) 'Conquering ammonium bisulfate poison over low temperature NH_3-SCR catalysts: A critical review', Applied Catalysis B: Environmental, 297, 120388. doi: 10.1016/j.apcatb.2021.120388.

Hadjiivanov, K. (2014) 'Identification and characterization of surface hydroxyl groups by infrared spectroscopy', Chemical Reviews, 100(11), pp. 3879–3894.

Hammershøi, P.S., Jangjou, Y., Epling, W.S., Jensen, A.D. and Janssens, T.V.W. (2018) 'Reversible and irreversible deactivation of Cu-CHA NH_3-SCR catalysts by SO_2 and SO_3', Applied Catalysis B: Environmental, 226, pp. 38–45. Available at: https://backend.orbit.dtu.dk/ws/files/140842370/1_s2.0_S0926337317311670_main.pdf

.

Hamzehlouyan, T., Sampara, C., Li, J., Kumar, A. and Epling, W. (2016) 'Sulfur poisoning of a Pt/Al_2O_3 oxidation catalyst: understanding of SO_2, SO_3 and H_2SO_4 impacts', Topics in Catalysis, 59(10), pp. 1028–1032. doi: 10.1007/s11244-016-0592-0.

Hansen, T.W., Delariva, A.T., Challa, S.R. and Datye, A.K. (2013) 'Sintering of catalytic nanoparticles: particle migration or Ostwald ripening?', Accounts of Chemical Research, 46(8), pp. 1720–1730.

He, J.-J. and Wang, C.-X. (2016) 'Thermally induced deactivation and the corresponding strategies for improving durability in automotive three-way catalysts: a review of latest developments and fundamentals', Johnson Matthey Technology Review, 60(3), pp. 196–203.

He, Z., Wang, Y., Liu, Y., Lian, L., Kong, D. and Zhao, Y. (2024) 'Recent advances in sulfur poisoning of selective catalytic reduction (SCR) denitration catalysts', Fuel, 365, 131126. doi: 10.1016/j.fuel.2024.131126.

Heck, R.M., Farrauto, R.J. and Gulati, S.T. (2002) Catalytic Air Pollution Control: Commercial Technology. 2nd edn. New York: Wiley-Interscience.

Heveling, J. (2012) ‘Heterogeneous catalytic chemistry by example of industrial applications’, Journal of Chemical Education, 89(12), pp. 1530–1536. doi: 10.1021/ed200816g.

Ho, P.H., Woo, J.W., Ilmasani, R.F., Han, J. and Olsson, L. (2021) ‘The role of Pd–Pt interactions in oxidation and sulfur resistance of diesel oxidation catalysts’, Industrial & Engineering Chemistry Research, 60(18), pp. 6596–6612. doi: 10.1021/acs.iecr.0c05622.

Honkanen, M., Torvela, T., Kärkkäinen, M., Kolli, T. and Huuhtanen, M. (2015) ‘Accelerated deactivation studies of a natural gas oxidation catalyst: noble metal sintering and the effect of atmosphere’, Applied Catalysis B: Environmental, 182, pp. 449–460.

Hughes, A.E. (2021) ‘Platinum group metals: a review of resources and applications’, Resources, 10(9), p. 93. doi: 10.3390/resources10090093.

IEA (2021) Biofuels for Transport: Technology Roadmap. Paris: International Energy Agency. Available at: https://www.iea.org/reports/technology-roadmap-biofuels-for-transport (Accessed: 4 July 2025).

IEA (2022) Energy Efficiency 2022. Paris: International Energy Agency.

IEA (2023) Greenhouse Gas Emissions from Energy: Overview. Paris: International Energy Agency. Available at: https://iea.blob.core.windows.net/assets/f535fcce-abe8-49ff-9cc9-5c1d9d6eec07/WORLD_GHG_Documentation.pdf (Accessed: 2 July 2025).

Isahak, W.N.R.W. and Al-Amiery, A.A.H. (2024) ‘Catalysts driving efficiency and innovation in thermal reactions: A comprehensive review’, Green Energy & Sustainability [online]. doi: 10.1016/j.grets.2024.100078.

Iwamoto, M. and Hamada, H. (1991) ‘Removal of nitrogen monoxide from exhaust gases through selective catalytic reduction’, Catalysis Today, 10, pp. 57–71.

Jabłońska, M. (2022) ‘Review of the application of Cu-containing SSZ-13 in NH_3-SCR-DeNOx and NH_3-SCO’, Materials, 15, p. 1234.

Jenkins, R. and Snyder, R.L. (1996) Introduction to X-ray Powder Diffractometry. New York: Wiley.

Jeswani, H.K., Chilvers, A. and Azapagic, A. (2020) ‘Environmental sustainability of biofuels: A review of life cycle assessments’, Proceedings of the Royal Society A, 476(2234), p. 20200351. Available at: https://royalsocietypublishing.org/doi/10.1098/rspa.2020.0351 (Accessed: 4 July 2025).

Jiang, B., Liu, Y. and Wu, Z. (2016) ‘Low-temperature selective catalytic reduction of NO with NH_3 over Cu-based zeolite catalysts: A review’, Applied Catalysis B: Environmental, 199, pp. 93–109. doi: 10.1016/j.apcatb.2016.06.050.

Karre, A.V., Garlapalli, R.K., Jena, A. and Tripathi, N. (2023) ‘State of the art developments in oxidation performance and deactivation of diesel oxidation catalyst (DOC)’, Catalysis Communications, 179, 106682. Available at: https://www.sciencedirect.com/science/article/pii/S1566736723000845.

Kašpar, J., Fornasiero, P. and Hickey, N. (2003) ‘Automotive catalytic converters: current status and some perspectives’, Catalysis Today, 77, pp. 419–449.

Kaunisto, K., Hyvärinen, L., Keskinen, J. and Huttunen-Saarivirta, E. (2023) ‘Evolution of alumina phase structure in thermal plasma processing’, Ceramics International, 49(20), pp. 33236–33248.

Kim, C.H., Lee, J.H. and Peden, C.H.F. (2021) ‘Recent advances in automotive three-way catalyst technology: Pd-rich catalyst systems and hydrothermal stability’, Applied Catalysis B: Environmental, 284, 119700. doi: 10.1016/j.apcatb.2020.119700.

Kim, C.H., Parrish, M., Kwak, J.H., Szanyi, J. and Peden, C.H.F. (2022) ‘Deactivation and durability challenges of modern automotive emission control catalysts’, Catalysis Today, 384–386, pp. 3–15. doi: 10.1016/j.cattod.2021.09.015.

Kirchherr, J., Reike, D. and Hekkert, M. (2017) ‘Conceptualizing the circular economy: An analysis of 114 definitions’, Resources, Conservation & Recycling, 127, pp. 221–232.

Koebel, M., Elsener, M. and Kleemann, M. (2000) ‘Urea-SCR: a promising technique to reduce NOx emissions from automotive diesel engines’, Catalysis Today, 59(3–4), pp. 335–345. doi: 10.1016/S0920-5861(00)00299-6.

Kritsanaviparkporn, E. and Tsolakis, A. (2021) ‘Catalytic converters for vehicle exhaust: fundamental aspects and technology overview’, Vehicles, 3(2), pp. 305–334.

Kröger, V. (2016) ‘Poisoning of automotive exhaust gas catalyst components. The role of phosphorus in the poisoning phenomena.’ Doctoral thesis. Oulu: University of Oulu. Available at: https://oulurepo.oulu.fi/bitstream/handle/10024/34640/isbn978-951-42-8608-7.pdf (Accessed: 9 March 2026).

Kärkkäinen, M.-L. (2017) ‘Deactivation of oxidation catalysts by sulphur and phosphorus in diesel and gas driven vehicles.’ Doctoral thesis. Oulu: University of Oulu. Available at: https://oulurepo.oulu.fi/bitstream/handle/10024/34374/isbn978-952-62-1723-9.pdf (Accessed: 9 March 2026).

Lai, J.-K. and Wachs, I.E. (2018) ‘A perspective on the SCR of NO with NH_3 by supported V_2O_5–WO_3/TiO_2 catalysts’, ACS Catalysis, 8(7), pp. 6537–6551. doi: 10.1021/acscatal.8b01357.

Lambert, C.K. (2004) ‘Mechanisms of sulfur poisoning in automotive catalysts’, SAE Technical Paper, 2004-01-1293. doi: 10.4271/2004-01-1293.

Lee, H., Song, I., Jeon, S.W., Hwang, K.H. and Kim, D.H. (2024) ‘Regeneration of a sulfur-poisoned selective catalytic reduction catalyst at ambient conditions’, Applied Catalysis B: Environmental, 341, 123333. doi: 10.1016/j.apcatb.2023.123333.

Li, J.H., Chang, H.Z., Ma, L., Hao, J.M. and Yang, R.T. (2011) ‘Low-temperature selective catalytic reduction of NOx with NH_3 over metal oxide and zeolite catalysts—A review’, Catalysis Today, 175(1), pp. 147–156.

Li, J., Liu, X., Zhan, W., Guo, Y., Guo, Y. and Lu, G. (2016) ‘Preparation of high oxygen storage capacity and thermally stable ceria–zirconia solid solution’, Catalysis Science & Technology, 6(3), pp. 897–907. doi: 10.1039/C5CY01571E.

Li, C., Shen, M., Yu, T., Wang, J., Wang, J. and Zhai, Y. (2017) ‘The mechanism of ammonium bisulfate formation and decomposition over V/WTi catalysts for NH_3-selective catalytic reduction’, Physical Chemistry Chemical Physics, 19, pp. 15194–15203. doi: 10.1039/C7CP02324C.

Li, Z., Chen, G., Shao, Z., Zhang, H. and Guo, X. (2022a) ‘Effect of iron content on the NH_3-SCR performance of Fe-based catalysts’, Catalysts, 12(9), Article 969.

Li, P., Xin, Y., Zhang, H., Yang, F., Tang, A., Han, D., Jia, J., Wang, J., Li, Z. and Zhang, Z. (2022b) ‘Recent progress in performance optimization of Cu-SSZ-13 catalysts for NH_3-SCR of NOx: active sites, hydrothermal aging and deactivation’, Frontiers in Chemistry, 10, 1033255.

Lietti, L., Nova, I., Forzatti, P. and Tronconi, E. (1996) ‘Role of sulfur in the deactivation of commercial diesel oxidation catalysts’, Applied Catalysis B: Environmental, 10, pp. 281–297.

Lin, F., Xu, M., Ramasamy K. K., Li, Z., Klinger, J.L., Schaidle, J.A., Wang, H. (2022) ‘Catalyst deactivation and its mitigation during catalytic conversions of biomass’, ACS Catalysis [online]. doi: 10.1021/acscatal.2c02074.

Liu, Z., Woo, S.I. and Nam, I.S. (2010) ‘Sulfur tolerance of SCR catalysts and the role of sulfate formation’, Catalysis Surveys from Asia, 14, pp. 1–12. doi: 10.1007/s10563-009-9083-3.

Liu, Q., Ming, S., Bian, C. and Li, T. (2020) ‘The opportunities and challenges of iron-zeolite as NH_3-SCR catalyst in purification of vehicle exhaust’, Fuel, 279, 118577. doi: 10.1016/j.fuel.2020.118577.

Lisi, L. and Cimino, S. (2020) ‘Poisoning of SCR catalysts by alkali and alkaline earth metals’, Catalysts, 10(12), 1475. Available at: https://www.mdpi.com/2073-4344/10/12/1475.

Liu, Z.G., Ottinger, N.A. and Creemens, C. (2015) ‘Vanadium and tungsten release from V-based SCR catalysts under various conditions’, Journal of Hazardous Materials, 295, pp. 71–79.

Liu, Q., Wang, D., Li, J. and Woo, S.I. (2020) ‘The opportunities and challenges of iron-zeolite as NH_3-SCR catalysts: activity, stability and deactivation mechanisms’, Fuel Processing Technology, 206, 106466. doi: 10.1016/j.fuproc.2020.106466.

Ma, Z., Wu, X., Si, Z., Weng, D., Ma, J. and Xu, T. (2012) ‘Impacts of sulfur poisoning on Fe-based SCR catalysts’, Applied Catalysis B: Environmental, 119–120, pp. 52–60. doi: 10.1016/j.apcatb.2012.02.023.

Ma, J., Wang, C., Liu, X. et al. (2022) ‘Research progress on sulfur deactivation and regeneration over Cu-CHA zeolite catalyst’, Catalysts, 12(12), p. 1499. doi: 10.3390/catal12121499.

Maunula, T., Kallinen, K., Wolff, T. and Mikulski, M. (2025) ‘Catalytic aftertreatment systems for combustion exhaust gases from future hydrogen, ammonia and e-HC engines’, Topics in Catalysis, 68, pp. 2565–2580.

Meißner, J., Ahrens, L., Pasel, J., Schwedt, A., Wohlrab, S., Mayer, J. and Peters, R. (2023) ‘An improved preparation method for a CuO/CeO_2 coated monolith for the CO–PrOx reaction’, Scientific Reports, 13, Article 9345. doi: 10.1038/s41598-023-36423-7.

Mendoza Suarez, F. and Tatarchuk, B. (2025) ‘Comparative economic analysis of batch vs continuous manufacturing in catalytic heterogeneous processes: impact of catalyst activity maintenance and materials costs on total costs of manufacturing in the production of fine chemicals and pharmaceuticals’, Journal of Flow Chemistry, 15, pp. 21–38.

Miao, J., Li, J., Qi, G. and Li, W. (2020) ‘Poisoning effects of phosphorus, potassium and lead on V_2O_5–WO_3/TiO_2 catalysts for selective catalytic reduction with NH_3’, Catalysts, 10(3), p. 345. Available at: https://www.mdpi.com/2073-4344/10/3/345.

Ministry of Economic Affairs and Employment of Finland (2022) National Climate and Energy Strategy. Helsinki: Ministry of Economic Affairs and Employment of Finland. Available at: https://julkaisut.valtioneuvosto.fi/handle/10024/164323 (Accessed: 2 July 2025).

Montanari, T., Marie, O., Daturi, M. and Busca, G. (2007) ‘Searching for the active sites of Co-H-MFI catalyst for the selective catalytic reduction of NO by methane: a FT-IR in situ and operando study’, Applied Catalysis B: Environmental, 71(3–4), pp. 216–222. doi: 10.1016/j.apcatb.2006.09.010.

Moulijn, J.A., Makkee, M. and Van Diepen, A.E. (2013) Chemical Process Technology. 2nd edn. Chichester: Wiley.

Mu, X. (2025) ‘Research progress on zeolite-type high-temperature NH_3-SCR catalysts’, Catalysts [online]. Available at: https://www.mdpi.com/2073-4344/15/11/1060 (Accessed: 10 February 2026).

Nasir, J.A. (2024) ‘Mechanistic insights into transition metal zeolite catalysts for NH_3-SCR’, Catalysis Science & Technology [online]. Available at: https://pubs.rsc.org/en/content/articlehtml/2024/cs/d3cs00468f (Accessed: 10 February 2026).

Nova, I. and Tronconi, E. (2014) Urea-SCR Technology for DeNOx After Treatment of Diesel Exhausts. New York: Springer.

OECD (2019) Global Waste Management Outlook. Paris: OECD Publishing.

Olsen, B.K., Kügler, F., Castellino, F. and Jensen, A.D. (2016) ‘Poisoning of vanadia based SCR catalysts by potassium: influence of catalyst composition and potassium mobility’, Catalysis Science & Technology, 6, pp. 2249–2260. doi: 10.1039/c5cy01409c.

Padder, S.A., Rafiq, S., Mir, M.A., Alam, T. and Altaf, A. (2024) 'Biofuel generations: new insights into challenges and advancements', Biomass and Bioenergy, 180, 107358. Available at: https://www.sciencedirect.com/science/article/abs/pii/S0961953424001739 (Accessed: 4 July 2025).

Pan, W., Zhang, T., Li, X. and Chen, L. (2023) 'Research progress of the selective catalytic reduction with NH_3 over ZSM-5 zeolite catalysts for NOx removal', Catalysts, 13(10), p. 1381. doi: 10.3390/catal13101381.

Paolucci, C., Khurana, I., Parekh, A.A., Li, S., Shih, A.J., Li, H., Di Iorio, J.R., Albarracin-Caballero, J.D., Yezerets, A., Miller, J.T., Delgass, W.N., Ribeiro, F.H., Gounder, R. and Peden, C.H.F. (2017) 'Dynamic multinuclear sites formed by mobilized copper ions in NOx selective catalytic reduction', Science, 357(6354), pp. 898–903. doi: 10.1126/science.aam7093.

Park, E.D. (2024) 'Recent progress on selective catalytic reduction of NOx with NH_3', Catalysts, 14(10), p. 1381. doi: 10.3390/catal14101381.

Peng, Y., Li, J., Si, W., Luo, J. and Dai, Q. (2015) 'Deactivation mechanism of alkali metals on Fe-based SCR catalysts', Environmental Science & Technology, 49, pp. 12603–12611. doi: 10.1021/acs.est.5b03051.

Pham, P.T.H., Pham, C.Q., Dam, T.-T., Nguyen, Q.-A. and Nguyen, T.M. (2024) 'A comprehensive review of catalyst deactivation and regeneration in industrial catalysis', Chemical Engineering Journal, 475, 147284.

Pinciroli, L., Baraldi, P., Zio, E. (2023) 'Maintenance optimization in Industry 4.0', Reliability Engineering & System Safety, 233.

Putluru, S.S.R., Jensen, A.D., Riisager, A. and Fehrmann, R. (2011) 'Alkali resistant Fe-zeolite catalysts for SCR of NO with NH_3 in flue gases', Topics in Catalysis, 54(14), pp. 1286–1292. doi: 10.1007/s11244-011-9750-6.

Qi, C., Bao, W., Wang, L., Li, H., Wu, W. (2017) 'Study of the V_2O_5–WO_3/TiO_2 catalyst synthesized from waste catalyst on selective catalytic reduction of NOx by NH_3', Catalysts, 7(4), p. 110.

Qian, X., Ao, W., Ding, H., Wang, X., Sun, S. (2022a) 'A review on resource utilization of spent V–W–Ti based selective catalytic reduction catalysts', Materials, 15(22), p. 7984.

Qian, K., Li, X., Chen, H., Liu, Z., Ma, J. and He, H. (2022b) 'Deactivation and regeneration of NH_3-SCR catalysts for NOx removal: a review', Chemical Engineering Journal, 446, 137341. doi: 10.1016/j.cej.2022.137341.

Qiu, Y., Fan, C., Sun, C., Zhu, H., Yi, W., Chen, J., Guo, L., Niu, X., Chen, J., Li, J. (2020) 'New insight into the in situ SO_2 poisoning mechanism over Cu-SSZ-13 for NH_3-SCR', Catalysts, 10, p. 1391.

Ravindran, K. and Madhu, G. (2020) 'Impact of shape and size of catalysts on the physical properties and pressure drop in fixed bed catalytic systems', International Journal of Innovative Technology and Exploring Engineering, 9(6), pp. 1103–1108. Available at: https://www.researchgate.net/publication/356345185 (Accessed: 26 July 2025).

Richardson, J.T. (1989) Principles of Catalyst Development. New York: Plenum Press. Available at: https://link.springer.com/book/10.1007/978-1-4899-3725-4(Accessed: 14 July 2025).

Rood, S., Eslava, S., Manigrasso, A. and Bannister, C. (2019) 'Recent advances in gasoline three way catalyst formulation: a review', Journal of Automobile Engineering, 233(12), pp. 2987–3001. doi: 10.1177/0954407019859822.

Russell, A. and Epling, W. (2011) 'Diesel oxidation catalysts', Catalysis Reviews, 53(4), pp. 337–423. doi: 10.1080/01614940.2011.596429.

Sabatini, T., Onori, S., Nasti, T., Bongiorno, C., Raffaele, M. and Maggiore, R. (2016) 'Characterization of aging effect on three-way catalyst oxygen storage dynamics', SAE Technical Paper, 2016-01-0971.

Sandhu, N., Yu, X. and Zheng, M. (2024) ‘Catalytic NO_x aftertreatment — towards ultra-low NO_x mobility’, International Journal of Automotive Manufacturing and Materials.

Schlumberger, C. and Thommes, M. (2021) ‘Characterization of hierarchically ordered porous materials by physisorption and mercury porosimetry: a tutorial review’, Advanced Materials Interfaces, 8(4), 2002181. doi: 10.1002/admi.202002181.

Schlögl, R. (2015) ‘Heterogeneous catalysis’, Angewandte Chemie International Edition, 54(11), pp. 3465–3520. doi: 10.1002/anie.201410738.

Sheldon, R.A. and Brady, D. (2018) ‘The limits to biocatalysis: pushing the envelope’, Chemical Communications, 55, pp. 1704–1719.

Shelef, M. and McCabe, R.W. (2000) ‘Twenty-five years after introduction of automotive catalysts: what next?’, Catalysis Today, 62(1), pp. 35–50. doi: 10.1016/S0920-5861(00)00407-7.

Shen, M., Wang, Z., Li, X., Wang, J., Wang, J., Wang, C., Wang, J. (2019) ‘Effects of regeneration conditions on sulfated CuSSZ-13 catalysts for NH_3-SCR’, Korean Journal of Chemical Engineering.

Shi, Y., Wang, X., Chen, L., Li, S., Wu, C., Shan, S., Li, W. (2020) ‘In situ DRIFT study on NH_3 selective catalytic reduction of NOx by ammonia over oxide catalysts: mechanistic insights’, Applied Catalysis B: Environmental.

Shwan, S., Skoglundh, M., Fridell, E. and Jansson, J. (2014b) ‘Phosphorus deactivation of Fe-BEA catalyst for NH_3-SCR’, Applied Catalysis B: Environmental, 150–151, pp. 111–120. doi: 10.1016/j.apcatb.2013.12.028.

Shwan, S., Jansson, J., Olsson, L. and Skoglundh, M. (2015a) ‘Chemical deactivation of H-BEA and Fe-BEA as NH_3-SCR catalysts—effect of potassium’, Applied Catalysis B: Environmental, 166–167, pp. 277–286.

Shwan, S., Jansson, J., Olsson, L. and Skoglundh, M. (2015b) ‘NH_3-SCR activity of H-BEA and Fe-BEA after potassium exposure’, Topics in Catalysis, 58(14–17), pp. 1012–1018.

Song, I., Lee, H., Jeon, S.W., Ibrahim, I.A.M., Kim, J., Byun, Y., Koh, D.J., Han, J.W., Kim, D.H. (2021) 'Simple physical mixing of zeolite prevents sulfur deactivation of vanadia catalysts for NOx removal', Nature Communications, 12, Article 838.

Theis, J.R., Lambert, C.K., McCabe, R.W. and Farrauto, R.J. (2001) 'Sulfur and phosphorus poisoning of automotive catalysts', Catalysis Today, 67–68, pp. 3–14.

Thomas, J.M. and Thomas, W.J. (2015) Principles and Practice of Heterogeneous Catalysis. Weinheim: Wiley-VCH.

Thommes, M., Kaneko, K., Neimark, A.V., Olivier, J.P., Rodriguez-Reinoso, F., Rouquerol, J. and Sing, K.S.W. (2015) 'Physisorption of gases, with special reference to the evaluation of surface area and pore size distribution', Pure and Applied Chemistry, 87(9–10), pp. 1051–1069. doi: 10.1515/pac-2014-1117.

Twigg, M.V. (2007) Catalyst Handbook. 2nd edn. Boca Raton, FL: CRC Press. Available at: https://www.routledge.com/Catalyst-Handbook/Twigg/p/book/9780849391591 (Accessed: 15 July 2025).

Twigg, M.V. (2011) 'Progress and future challenges in controlling automotive exhaust gas emissions', Applied Catalysis B: Environmental, 70(1–4), pp. 2–15. doi: 10.1016/j.apcatb.2005.02.029.

Ulusoy, U. (2023) 'A review of particle shape effects on material properties for various engineering applications: from macro to nanoscale', Minerals, 13(1), p. 91. doi: 10.3390/min13010091.

van der Bij, H.E. and Weckhuysen, B.M. (2015) 'Phosphorus promotion and poisoning in zeolite-based materials: synthesis, characterisation and catalysis', Chemical Society Reviews, 44(21), pp. 7406–7428.

Velichkina, L., Barbashin, Y., Vosmerikov, A. (2021) 'Effect of acid treatment on the properties of zeolite catalyst fpr straight-run gasoline upgrading', Catalysis Research.

Väliheikki, A. (2016) 'Resistance of catalytic materials towards chemical impurities: The effect of sulphur and biomaterial-based compounds on the performance of DOC and SCR

catalysts.' Doctoral thesis. Oulu: University of Oulu. Available at: https://oulurepo.oulu.fi/handle/10024/34792 (Accessed: 9 July 2025).

Wang, Y., Liu, G., Qi, G., Pan, H., Wang, Z. and Li, J. (2019) 'Deactivation and regeneration for the SO_2-poisoning of a Cu-CHA catalyst in the NH_3-SCR reaction', Catalysts, 9, p. 797.

Wang, A., Li, J., Liu, Z., Chen, H. et al. (2020) 'A deactivation mechanism study of phosphorus-poisoned diesel oxidation catalysts: model and supplier catalysts', Catalysis Science & Technology, 10, pp. 5320–5334. doi: 10.1039/D0CY00589D.

Wang, B., Zhang, Y. and Xiaolei, F. (2023) 'Deactivation of Cu SCR catalysts based on small-pore SSZ: a review', Cambridge Publications Index.

World Commission on Environment and Development (1987) Our Common Future. Oxford: Oxford University Press.

Wu, D., Zhou, J. and Li, Y. (2007) 'Mechanical strength of solid catalysts: recent developments and future prospects', AIChE Journal, 53(10), pp. 2618–2629. doi: 10.1002/aic.11291.

Xu, D., Qu, W., Liu, J., Chen, J., Fang, X., Chen, L., Ma, Z., Liu, X., Tang, X. and Chen, Y. (2023) 'Active sites of NO selective catalytic reduction over V_2O_5–WO_3/TiO_2', Journal of Materials Chemistry A, 11, pp. 24644–24650. doi: 10.1039/D3TA05525F.

Xiao, H. (2018) 'Influence of sulfur-containing sodium salt poisoned V_2O_5–WO_3/TiO_2 catalysts', Catalysts, 8(11), p. 541. doi: 10.3390/catal8110541.

Xie, Y., Muncrief, R., Minjares, R. and Rodríguez, F. (2020) Diesel sulfur content impacts on Euro VI soot-free vehicles. International Council on Clean Transportation.

Yakoumis, I. (2023) 'Innovative technologies for the recovery of platinum group metals from spent automotive catalysts', Gospodarka Surowcami Mineralnymi – Mineral Resources Management, 39(2), pp. 5–24. doi: 10.24425/gsm.2023.146001.

Yang, S., Wang, C., Li, J., Yan, N., Ma, L. and Chang, H. (2015) 'Mechanistic insights into NH_3-SCR over Fe-based catalysts from in situ DRIFTS studies', Catalysts, 5, pp. 196–218.

Yang, W., Gong, J., Wang, X., Bao, Z., Guo, Y. and Wu, Z. (2021) 'A review on the impact of SO_2 on the oxidation of NO, hydrocarbons, and CO in diesel emission control catalysis', ACS Catalysis, 11(20), pp. 12446–12468. doi: 10.1021/acscatal.1c03013.

Ye, B., Jeong, B., Lee, M., Kim, T.H., Park, S.S., Jung, J., Lee, S. and Kim, H.D. (2022) 'Recent trends in vanadium-based SCR catalysts for NO_x reduction in industrial applications: stationary sources', Nano Convergence, 9, p. 51. doi: 10.1186/s40580-022-00341-7.

Yu, D., Wang, P., Li, X., Zhao, H. and Lv, X. (2023) 'Study on the role of Fe species and acid sites in NH_3-SCR over Fe-based zeolites', Fuel, 336, 126759. doi: 10.1016/j.fuel.2022.126759.

Yu, Y., He, C., Deng, C., Wu, J. and Chen, J. (2019) 'SO_2 promoted in situ recovery of thermally deactivated Fe-based NH_3-SCR catalysts', Chemical Engineering Journal. Available at: https://orca.cardiff.ac.uk/id/eprint/122297/1/Postprint.pdf.

Zhang, D., Zhang, R., Liu, Z. and Wang, Y. (2018) 'N_2O formation pathways over zeolite-supported Cu and Fe catalysts during NH_3-SCR: mechanistic insights', Energy & Fuels, 32(10), pp. 10143–10156. doi: 10.1021/acs.energyfuels.7b03405.

Zhang, L., Li, J. and Ge, M. (2019) 'Sulfur resistance of Fe-based SCR catalysts: a review', Catalysts, 9(3), p. 234. doi: 10.3390/catal9030234.

Zhang, W., Qi, S., Pantaleo, G. and Liotta, L.F. (2019) 'WO_3–V_2O_5 active oxides for NOx SCR by NH_3: preparation methods, catalysts' composition, and deactivation mechanism — a review', Catalysts, 9(6), p. 527. doi: 10.3390/catal9060527.

Zhang, Z., Tian, J., Li, J., Cao, C., Wang, S., Lv, J., Zheng, W. and Tan, D. (2022) 'The development of diesel oxidation catalysts and sulfur effects on Pt/Pd catalysts', Fuel Processing Technology, 233, 107317. doi: 10.1016/j.fuproc.2022.107317.

Zhang, R., Xu, D., Qu, W., Liu, J. and Chen, Y. (2024a) ‘Vanadium-based catalysts for selective catalytic reduction of NOx with ammonia: synthesis, poisoning mechanism, regeneration methods and research prospects’, Fuel, 365, 131184.

Zhang, T. (2024b) ‘Deterioration analysis of real-world SCR catalysts’, International Journal of Advanced Materials and Manufacturing, 3(4), pp. 1–12.

Zhang, Y. (2024c) ‘Research on the resistance of catalysts for selective catalytic reduction (SCR) technology’, Journal of Cleaner Production.

Zhao, Y., Wang, X. and Li, J. (2021) ‘Coupled thermal and chemical aging of three-way catalysts’, Applied Catalysis B: Environmental, 297, 120474.

Zhao, L., Zhang, Y. and Kang, M. (2022) ‘Recent advances in heightening sulphur resistance of SCR catalysts: a review’, Environmental Engineering Research, 27(1), p. 200642. doi: 10.4491/eer.2020.642.

Zhao, J., Zhang, X., Yang, F., Ai, Y., Chen, Y., Pan, D. (2024) ‘Strategy and technical progress of recycling of spent vanadium–titanium SCR catalysts’, Materials.

Zhu, N., Liu, S., Wang, Y., Hao, J. and Liu, F. (2020) ‘Effects of alkali and alkaline earth metals on Cu-SSZ-39 SCR catalysts’, Chemical Engineering Journal, 396, 125270. doi: 10.1016/j.cej.2020.125270.

APPENDIX 1: ACTIVITY MEASUREMENTS

Detailed concentrations of the individual deactivated catalysts experiments.

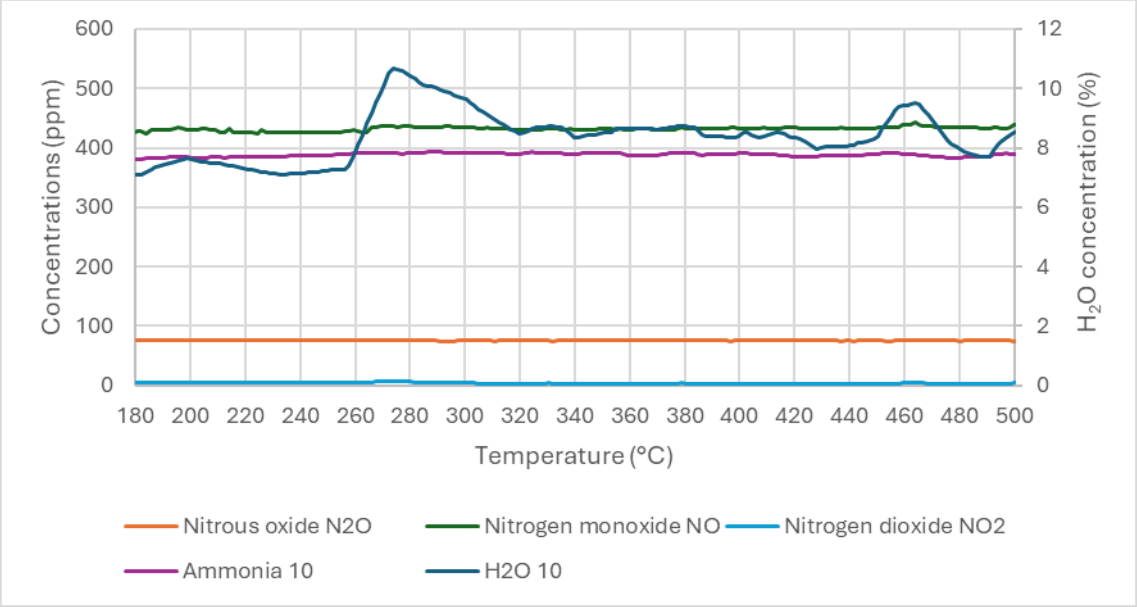

Figure A1. Blank test without catalyst.

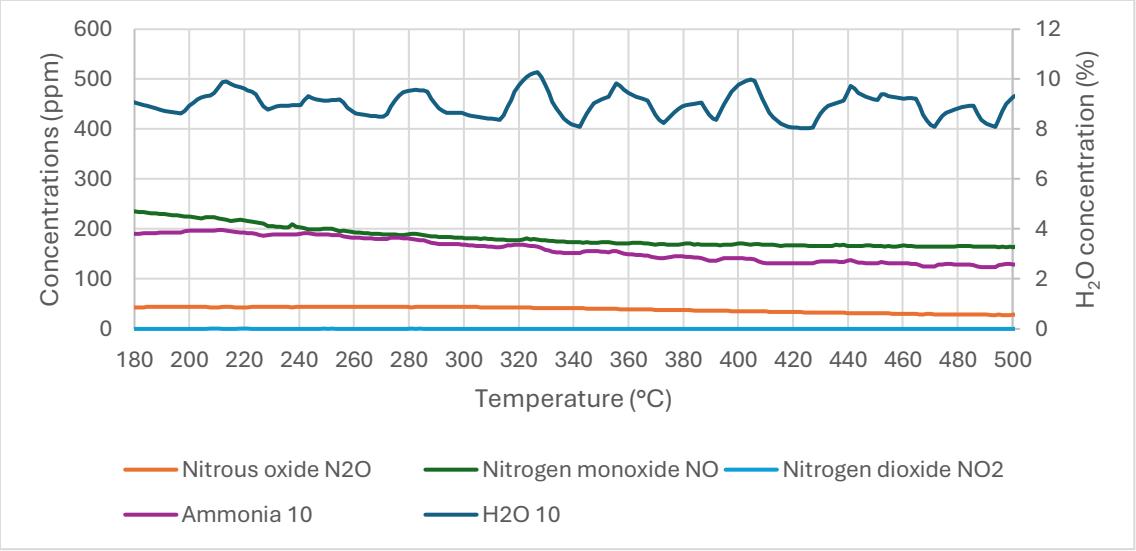

Figure A2. Hydrothermally treated Fe-SCR catalyst.

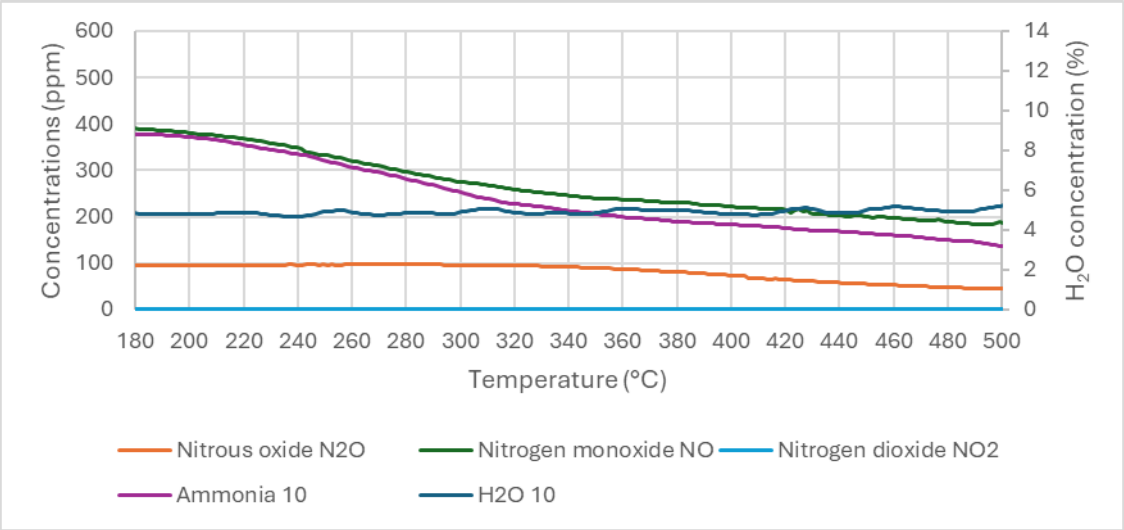

Figure A3. Fe-SCR catalyst treated hydrothermally with sulphur.

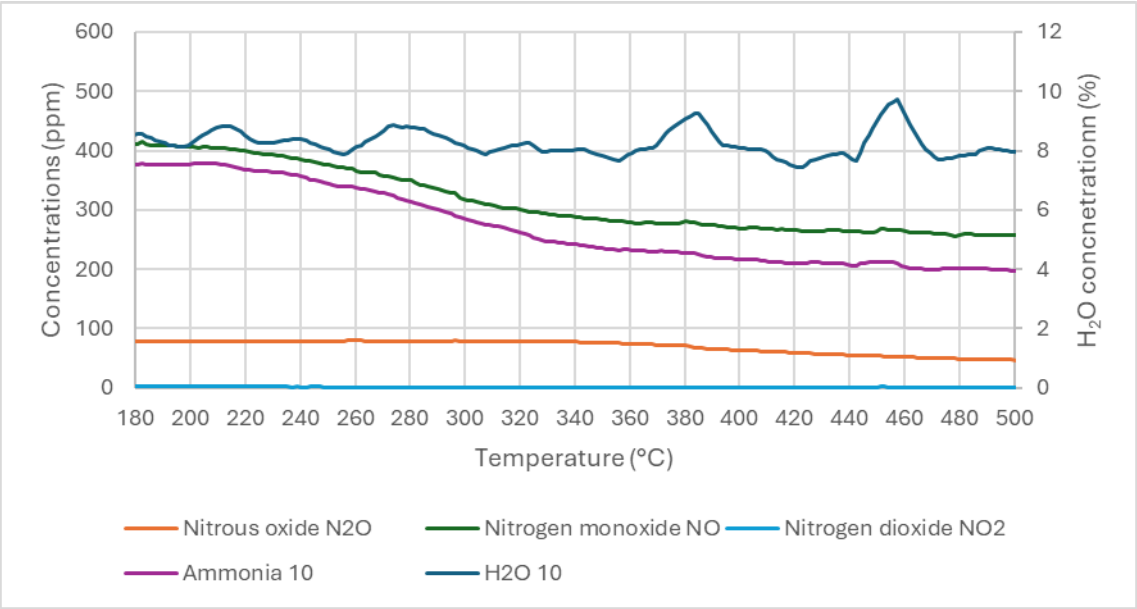

Figure A4. Fe-SCR catalyst treated hydrothermally with sulphur and potassium.

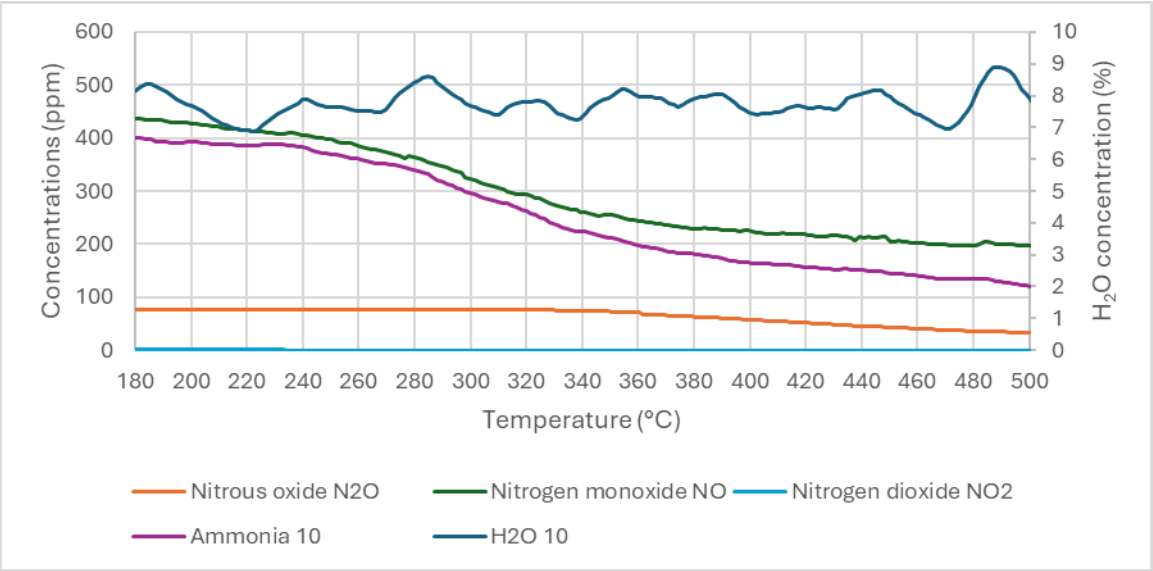

Figure A5. Fe-SCR catalyst treated hydrothermally with sulphur and calcium.

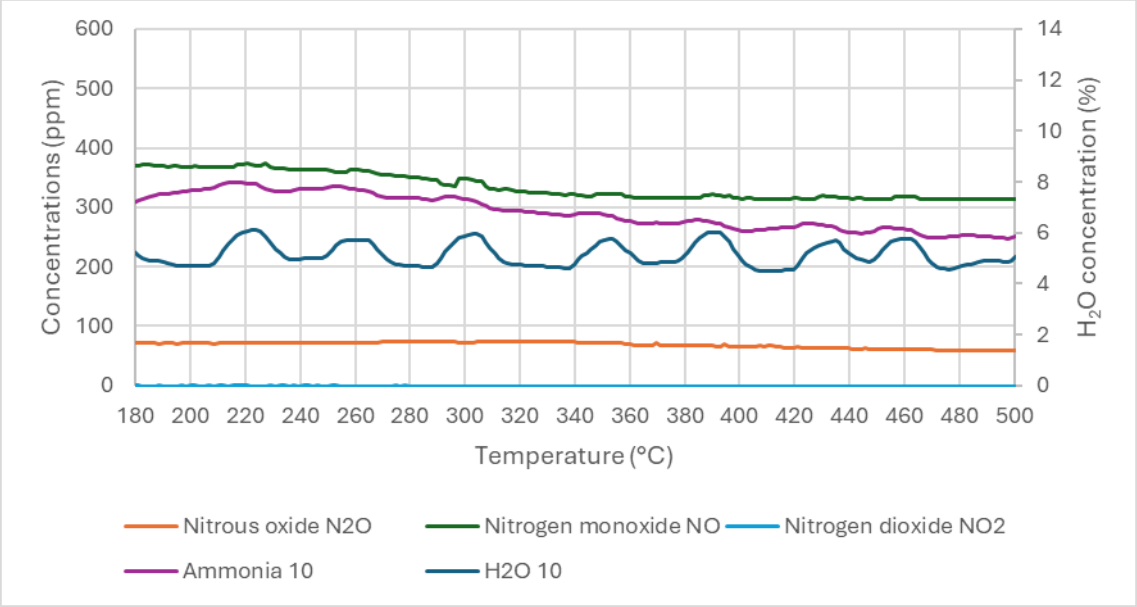

Figure A6. Fe-SCR catalyst treated hydrothermally with sulphur and sodium.

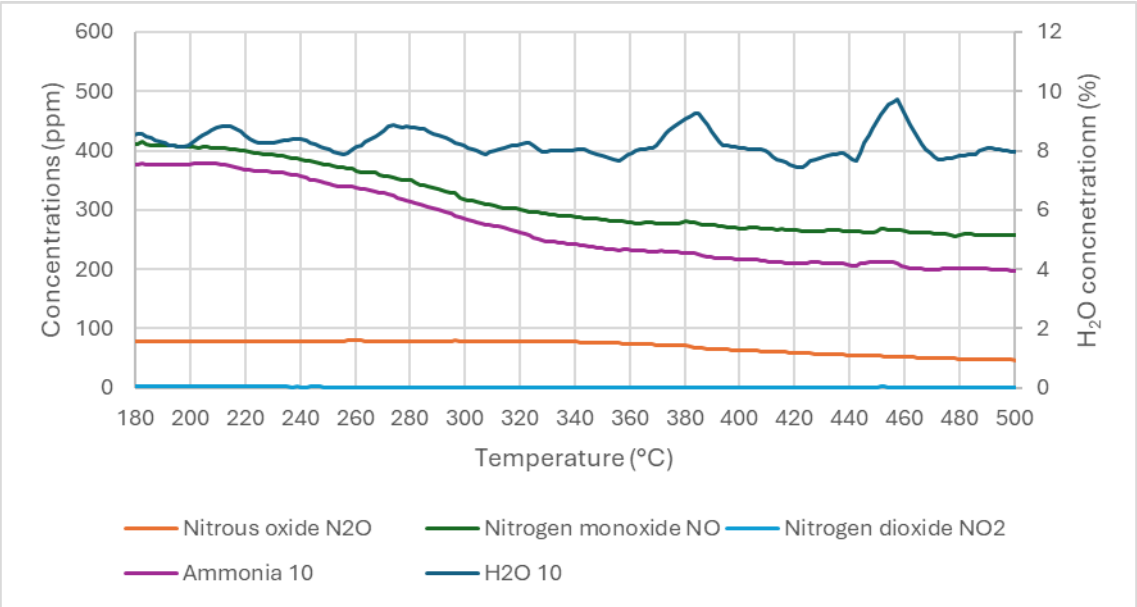

Figure A7. Fe-SCR catalyst treated hydrothermally with sulphur and phosphorus.